Physical-Layer Security of SIMO Communication Systems over Multipath Fading Conditions

Jules M. Moualeu, *Senior Member, IEEE*, Paschalis C. Sofotasios, *Senior Member, IEEE*, Daniel B. da Costa, *Senior Member, IEEE*, Sami Muhaidat, *Senior Member, IEEE*, Walaa Hamouda, *Senior Member, IEEE*, and Ugo S. Dias, *Senior Member, IEEE*

Abstract—The present work investigates the physical layer security of wireless communication systems over non-homogeneous fading environments, i.e. η-μ and λ-μ fading models, which are typically encountered in realistic wireless transmission scenarios in the context of conventional and emerging communication systems. This study considers a single-input multiple-output system that consists of a single-antenna transmitter, a multi-antenna legitimate receiver, and an active multi-antenna eavesdropper. To this end, novel exact analytical expressions are derived for the corresponding average secrecy capacity and secrecy outage probability, which are corroborated by respective results from computer simulations. Capitalizing on the offered results, the physical layer security is quantified in terms of different parameters, which leads to useful insights on the impact of non-homogeneous fading environment and the number of employed antennas on the achieved physical layer security levels of the underlying system configuration. The offered results and insights are useful for the design of such systems as well as for the computational requirements and sustainability relating to such systems, since emerging communications are largely characterized by stringent quality of service and complexity requirements.

Index Terms—Multipath fading, secrecy capacity, secrecy outage probability, physical layer security, multi-antenna communications, computational complexity.

1 Introduction

Physical layer (PHY) security has received a great deal of attention in the past few years since it can address the issues of privacy and security in wireless communication networks, without necessarily relying on encryption techniques. Owing to this fact, several reported contributions have investigated the secrecy performance over small-scale fading channels and large-scale fading channels ([1]–[6] and references therein). However, the aforementioned fading conditions do not typically encompass various fading types that are experienced in practical communication scenarios. This also concerns the effects of non-homogeneous fading environments such as α-μ [7], and κ-μ and η-μ [8], which although they are encountered in realistic communication scenarios, they are typically neglected for the sake of complexity reduction. As a result, several simplistic assumptions have led to results that are largely inaccurate, which is a critical issue in the context of secure communications since the reliability of modeling effects is of paramount importance. To this end, recent emphasis on generalized fading distributions that do not necessarily assume homogeneous fading environments has generated a considerable interest in analyses relating to PHY security, which constitutes a critical topic of interest in emerging communication technologies (see for instance, [9]–[18] and references therein). Specifically, the authors in [9] derived analytical expressions for the lower bound of the secrecy outage probability (SOP) and the probability of strictly positive secrecy capacity (SPSC) over generalized Gamma fading channels. Likewise, the secrecy performance analysis over generalized-K fading channels was investigated in [10], while the effects of κ-μ and α-μ fading conditions were investigated in [11] and in [12], respectively. Considering a different configuration from the above studies [9]–[12], the authors in [13]–[16] investigated the PHY security problem in a single-input multiple-output (SIMO) system over the generalized-K, κ-μ, κ-μ shadowed and α-μ fading channels, respectively. In [17], the secrecy performance of stochastic MIMO wireless networks over α-μ fading channels was studied in terms of the connection outage probability (COP), the probability of non-zero secrecy capacity (PNZ) and ergodic secrecy capacity. Most recently, a comprehensive and unifying fading model introduced in [19], i.e., the α-η-κ-μ distribution, was investigated in the context of secure wireless communication systems (e.g. [18]). In [18], the authors obtained novel and exact expressions for the secrecy performance metrics of the classic Wyner's wiretap model.

Other types of versatile fading distributions are the so-called η-μ and λ-μ fading models [8], [20], which can accurately model the small-scale variations of the wireless signal under non-line-of-sight conditions. The generality of these models is also evident by the fact that they include as special cases well-known multipath

J. M. Moualeu is with the School of Electrical and Information Engineering, University of the Witwatersrand, Johannesburg, 2000, South Africa, (email: jules.moualeu@wits.ac.za).
P. C. Sofotasios is with the Center for Cyber-Physical Systems, Department of Electrical and Computer Engineering, Khalifa University, Abu Dhabi 127788, United Arab Emirates, and also with the Department of Electrical Engineering, Tampere University, 33101 Tampere, Finland (e-mail: p.sofotasios@ieee.org).
D. B. da Costa is with Department of Computer Engineering, Federal University of Ceará, Sobral, CE, Brazil (email: danielbcosta@ieee.org).
S. Muhaidat is with the Center for Cyber-Physical Systems, Department of Electrical and Computer Engineering, Khalifa University, Abu Dhabi 127788, United Arab Emirates, and also with the Institute for Communication Systems, University of Surrey, Guildford GU2 7XH, U.K. (e-mail: muhaidat@ieee.org).
W. Hamouda is with the Department of Electrical and Computer Engineering, Concordia University, Montreal, QC H3G 1M8, Canada, (email: hamouda@ece.concordia.ca).
U. S. Dias with the Department of Electrical Engineering, University of Brasília, DF, Brazil (email: ugodias@ieee.org).
The work of J. M. Moualeu was supported in part by the NRF Funding Incentive for Rated Researchers. The work of P. C. Sofotasios and S. Muhaidat was supported in part by Khalifa University under Grant No. KU/RC1-C2PS-T2/8474000137 and Grant No. KU/FSU-8474000122.
This paper was presented in part at the IEEE International Conference on Advanced Communication Technologies and Networking (CommNet 2019)

fading models such as Rayleigh, Nakagami-m and Nakagami-q i.e. Hoyt distributions. Because of their wide applicability and versatility [8], their consideration in the context of PHY security arises as an interesting issue to be investigated. However, none of the above-cited works (i.e., [9]–[18]) has studied the performance analysis of secure wireless communication in either η-μ or λ-μ fading conditions. Importantly, it is expected that the proposed investigations will be also insightful in terms of the computational complexity and sustainability associated with the determination of secure communications in the context of emerging communication systems. Besides the traditional communication-based perspective, such insights on the related computations are of paramount importance since modern communication systems and networks are typically characterized by stringent quality of service requirements and increased computational complexity and costs, which render their sustainability a challenging task. Thus, the core aim of the present analysis is to provide the necessary tools for an in-depth quantification of the computational sustainability associated with physical layer security in emerging communications in realistic propagation media, which will be useful in the effective and sustainable deployment and operation of future communication systems, both independently and as part of the generic Internet of Things (IoT) paradigm.

To the best of the authors' knowledge, the secrecy performance of wireless communication systems over η-μ and λ-μ fading models remains vastly unexplored. Motivated by the above, the present work conducts an investigation into the physical layer security of SIMO systems under generalized multipath fading conditions characterized by η-μ and λ-μ distributed fading conditions. The main contributions of this work are as follows:

- Novel analytical expressions for ASC and the secrecy outage probability (SOP) of the considered setup are derived. These expressions are given in terms of infinite series representations, which are fully convergent and involve elementary and known special functions. Also, a small number of terms is required to ensure a sufficiently low truncation error.
- Simple closed-form upper bounds for the truncation errors of the involved infinite series are also derived in order to enable precise determination of the number of truncation terms required to achieve certain accuracies. The derived analytical expressions are subsequently employed to quantify the ASC and the SOP under the considered fading conditions.
- Simple and explicit expressions of the asymptotic SOP in the high-SNR regime are obtained under both the η-μ and λ-μ fading models.
- The validity of the offered results is verified through extensive comparisons with respective results from computer simulations. It is shown that the number of antennas is critical to the level of achieved security as it improves the performance when they increase at the legitimate user, and they degrade it as their number increases at the eavesdropper. Also, it is shown that the effects of non-homogeneous fading have a non-negligible effect on the ASC and SOP performance. However, the effect of fading conditions in both cases is, as expected, smaller when the number of antennas at the legitimate and at eavesdropper's links is not small.

The remainder of the paper is organized as follows: Section 2 describes the considered system and channel models, while Section 3 focuses on the analysis of the ASC over generalized multipath fading channels characterized by η-μ and λ-μ fading models. Likewise, the corresponding exact and asymptotic SOP under these fading conditions are analyzed in Section 4, followed by corresponding numerical results, and insightful discussions are provided in Section 5. Finally, concluding remarks are provided in Section 6.

2 System and Channel Models

As shown in Fig. 1, we consider a SIMO wiretap channel in which the transmitter (Alice) sends confidential messages to the legitimate receiver (Bob) with a transmit power denoted by P, while the eavesdropper (Eve) overhears the transmission through the eavesdropper channel. In this context, it is assumed that Alice is equipped with a single antenna whereas Bob and Eve are equipped with multiple antennas, denoted as L_B and L_E, respectively. Also, both the legitimate (Alice-Bob) channel and the eavesdropper (Alice-Eve) channel are assumed to undergo independent and identically distributed (i.i.d.) quasi-static generalized η-μ and λ-μ fading conditions. In this context, an active eavesdropping scenario is considered, in which the channel state information (CSI) of both the main and wiretap links are known at Alice. Also, a maximal-ratio combining (MRC) scheme is employed at the involved receivers in order to exploit the antenna diversity and to maximize the probabilities of secure transmission and successful eavesdropping. The latter probability represents the worst-case scenario in the context of physical layer security, and it is paramount to investigate wireless communication system under such circumstances.

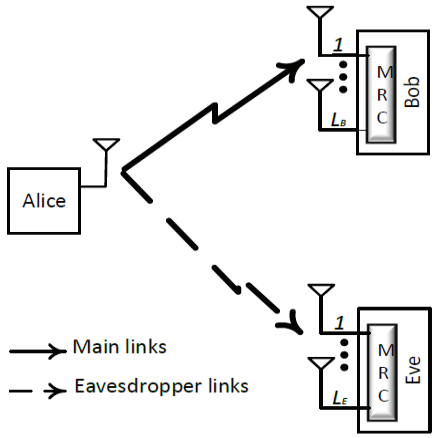

Fig. 1: Illustration of a SIMO wiretap channel, where a single-antenna transmitter (Alice) communicates with a multi-antenna legitimate receiver (Bob) in the presence of an active multi-antenna eavesdropper (Eve).

The encountered fading conditions in the underlying setup are assumed to be η-μ and λ-μ distributed with arbitrary values of fading parameters. These two models represent physical measures and have been distinct for their generality since they have been shown extensively, both theoretically and experimentally, capable of providing accurate characterization of versatile multipath fading channels [8], [20]–[22], and the references therein. Specifically, these fading models consider that the signals are composed of clusters of multipath waves propagating in a non-homogeneous environment. Within any one cluster, the phases of the scattered waves are random and have similar delay times with delay-time spreads of different clusters being relatively large. Furthermore, the in-phase and quadrature components of wireless signals within each cluster are assumed to: i) be independent to each other

and have different powers, in the η-μ fading model; ii) have zero mean and identical power but they are correlated, in the λ-μ fading model. In this context, μ represents the number of multipath clusters, in both fading models, η denotes the power ratio of the in-phase and quadrature components of the wireless signal within each cluster and λ denotes the correlation coefficient between the scattered-wave in-phase and quadrature components in each multipath cluster [8], [20]. Different from the η-μ and λ-μ fading models, the α-μ fading model accounts for the nonlinearity and clustering of a propagation channel, while the κ-μ fading distribution is better suited for line-of-sight (LOS) applications. In the former model, the nonlinearity is described in terms of a power parameter, so that the resulting signal intensity is obtained in two ways: (a) modulus of the sum of the multipath components, (b) modulus to a certain given exponent. In the latter model, each cluster of multipath waves is assumed to have scattered waves with identical powers and a dominant component found within.

The signal-to-noise ratio (SNR) probability density functions (PDF) of the η-μ and λ-μ fading distributions are obtained using [22, Eq. (1)] and [22, Eq. (2)], respectively and setting $\alpha = 1$, and are expressed as

$$\begin{aligned} f_\gamma(x) =& \frac{(\eta+1)^{\mu+\frac{1}{2}}\sqrt{\pi}\mu^{\mu+\frac{1}{2}}x^{\mu-\frac{1}{2}}}{\Gamma(\mu)\sqrt{\eta}(\eta-1)^{\mu-\frac{1}{2}}\overline{\gamma}^{\mu+\frac{1}{2}}} \\ & \times e^{-\frac{(1+\eta)^2\mu x}{2\eta\overline{\gamma}}} I_{\mu-\frac{1}{2}}\left(\frac{(\eta^2-1)\mu x}{2\eta\overline{\gamma}}\right), \end{aligned} \tag{1}$$

and

$$\begin{aligned} f_\gamma(x) =& \frac{(-1)^{\mu-\frac{1}{2}}2\sqrt{\pi}\mu^{\mu+\frac{1}{2}}x^{\mu-\frac{1}{2}}}{\Gamma(\mu)\sqrt{1-\lambda}\sqrt{1+\lambda}\lambda^{\mu-\frac{1}{2}}\overline{\gamma}^{\mu+\frac{1}{2}}} \\ & \times e^{-\frac{2\mu x}{(1-\lambda^2)}} I_{\mu-\frac{1}{2}}\left(\frac{2\lambda\mu x}{(\lambda+1)(\lambda-1)\overline{\gamma}}\right), \end{aligned} \tag{2}$$

where $\Gamma(\cdot)$ and $I_n(\cdot)$ denote the Euler Gamma function and the modified Bessel function of the first kind, respectively and $\bar{\gamma} = \mathbb{E}\{\gamma\}$ represents the average SNR, with $\mathbb{E}\{\cdot\}$ denoting statistical expectation. Based on the above representations and with the aid of [23, Eq. (8.445.1)] and [24], the corresponding PDFs of the SNR γ_i, $i \in \{B, E\}$[1], at the receiver's combiner output for each case are given by

$$\begin{aligned} f_{\gamma_i}(x) =& \sum_{k=0}^{\infty} \frac{2^{1-2L_i\mu_i-4k}(\eta_i+1)^{2L_i\mu_i}(1-\eta_i)^{2k}\mu_i^{2L_i\mu_i+2k}}{k!\eta_i^{L_i\mu_i+2k}\Gamma(L_i\mu_i)\Gamma\left(L_i\mu_i+k+\frac{1}{2}\right)} \\ & \times \frac{\sqrt{\pi}x^{2L_i\mu_i+2k-1}}{\bar{\gamma}_i^{2L_i\mu_i+2k}} e^{-\frac{2\mu_i(\eta_i+1)^2x}{4\eta_i\bar{\gamma}_i}}, \end{aligned} \tag{3}$$

and

$$\begin{aligned} f_{\gamma_i}(x) =& \sum_{k=0}^{\infty} \frac{2\sqrt{\pi}\lambda_i^{2k}\mu_i^{2L_i\mu_i+2k}}{k!(1-\lambda^2)^{L_i\mu_i+2k}\Gamma(L_i\mu_i)\Gamma\left(L_i\mu_i+k+\frac{1}{2}\right)} \\ & \times \frac{x^{2L_i\mu_i+2k-1}}{\bar{\gamma}_i^{2L_i\mu_i+2k}} e^{-\frac{2\mu_i x}{(1-\lambda)^2\bar{\gamma}_i}}, \end{aligned} \tag{4}$$

respectively. Based on (3) and (4), the corresponding cumulative distribution functions (CDF) are expressed as follows:

$$\begin{aligned} F_{\gamma_i}(x) =& \frac{\sqrt{\pi}\eta_i^{L_i\mu_i}}{2\Gamma(L_i\mu_i)(\eta_i+1)^{2L_i\mu_i}} \sum_{j=0}^{\infty} \frac{1}{j!2^{2j}\Gamma\left(L_i\mu_i+j+\frac{1}{2}\right)} \\ & \times \left(\frac{1-\eta_i}{1+\eta_i}\right)^{2j} \gamma_{\text{inc}}\left(2L_i\mu_i+2j, \frac{\mu_i(1+\eta_i)^2x}{2\eta_i\bar{\gamma}_i}\right), \end{aligned} \tag{5}$$

and

$$\begin{aligned} F_{\gamma_i}(x) =& \frac{\sqrt{\pi}(1-\lambda_i^2)^{L_i\mu_i}}{2^{2L_i\mu_i-1}\Gamma(L_i\mu_i)} \sum_{j=0}^{\infty} \frac{\lambda_i^{2j}}{j!2^{2j}\Gamma\left(L_i\mu_i+j+\frac{1}{2}\right)} \\ & \times \gamma_{\text{inc}}\left(2L_i\mu_i+2j, \frac{2\mu_i x}{(1-\lambda_i^2)\bar{\gamma}_i}\right), \end{aligned} \tag{6}$$

respectively, where $\gamma_{\text{inc}}(\alpha, x)$ denotes the lower incomplete Gamma function[2] [23, Eq. (8.350.1)].

3 Average Secrecy Capacity

In this section, the scenario wherein the CSI of the eavesdropper channel is available at Alice is considered. This scenario is applicable to wireless networks where Eve is active and Alice has access to her CSI [25]. In this case, a fundamental performance metric used to evaluate the secrecy performance is the ASC, which is defined as the instantaneous secrecy capacity C_S averaged over the instantaneous SNRs γ_B and γ_E, where $C_S = \max\{C_B - C_E, 0\}$ with $C_B = \log_2(1+\gamma_B)$ and $C_E = \log_2(1+\gamma_E)$ denoting the capacities of the main and eavesdropper channels, respectively. In what follows, we will determine the ASC for the case of $\eta-\mu$ and $\lambda-\mu$ fading conditions, which are encountered in practical communication scenarios.

3.1 Exact ASC over η-μ fading channels

It is recalled that the ASC can be formulated as follows:

$$\bar{C}_S = \int_0^\infty \int_0^\infty C_S f_{\gamma_B}(\gamma_B) f_{\gamma_E}(\gamma_E) \mathrm{d}\gamma_B \mathrm{d}\gamma_E \tag{7}$$

$$\begin{aligned} =& \underbrace{\frac{1}{\ln(2)} \int_0^\infty \ln(1+\gamma_B) f_{\gamma_B}(\gamma_B) F_{\gamma_E}(\gamma_B) \mathrm{d}\gamma_B}_{\mathcal{J}_1} \\ & + \underbrace{\frac{1}{\ln(2)} \int_0^\infty \ln(1+\gamma_E) f_{\gamma_E}(\gamma_E) F_{\gamma_B}(\gamma_E) \mathrm{d}\gamma_E}_{\mathcal{J}_2} \\ & - \underbrace{\frac{1}{\ln(2)} \int_0^\infty \ln(1+\gamma_E) f_{\gamma_E}(\gamma_E) \mathrm{d}\gamma_E}_{\mathcal{J}_3}. \end{aligned} \tag{8}$$

Based on this, the ASC in the considered set up for the case of η-μ fading conditions can be derived with the aid of the PDF and CDF representations in (3) and (5), respectively. To this end, it is evident that the ASC for the considered case can be obtained by deriving analytical expressions for the $\mathcal{J}_1^\eta$, $\mathcal{J}_2^\eta$ and $\mathcal{J}_3^\eta$ terms[3]

1. Henceforth, the subscript B is associated with Bob's measures, while the subscript E refers to Eve's measures.

2. The subscript "inc" is used in order to differentiate the instantaneous SNR γ_i from the lower incomplete Gamma function $\gamma_{\text{inc}}(\cdot,\cdot)$.

3. The $\mathcal{J}_n^\eta$ and $\mathcal{I}_n^\eta$ terms account for $\mathcal{J}_n$ and $\mathcal{I}_n$ for the case of η-μ fading channels, whereas the $\mathcal{J}_n^\lambda$ and $\mathcal{I}_n^\lambda$ terms account for $\mathcal{J}_n$ and $\mathcal{I}_n$ for the case of λ-μ fading channels.

Therefore, by substituting appropriately (3) and (5) into (8), the $\mathcal{J}_1^{\eta}$ term can be expressed as

$$\mathcal{J}_1^{\eta} = \frac{2^{1-2L_B\mu_B+2L_E\mu_E}\pi(\eta_B+1)^{2L_B\mu_B}}{\ln(2)\eta_B^{L_B\mu_B}\Gamma(L_B\mu_B)\Gamma(L_E\mu_E)\bar{\gamma}_B^{2L_B\mu_B}} \times \sum_{k=0}^{\infty}\sum_{j=0}^{\infty} \frac{\eta_E^{L_E\mu_E-2j}(1-\eta_E^2)^{2j}}{k!j!((\eta_E+1)^{2L_E\mu_E+4j}\bar{\gamma}_B^{2k}} \left(\frac{1-\eta_B^2}{4\eta_B}\right)^{2k} \times \frac{\mu_B^{2L_B\mu_B+2k}2^{1-2L_E\mu_E-2j}}{\Gamma(L_B\mu_B+k+0.5)\Gamma(L_E\mu_E+2j+0.5)} \times \int_0^{\infty} \frac{\ln(1+\gamma_B)\gamma_{\text{inc}}\left(2L_E\mu_E+2j, \mathcal{A}_E\gamma_B\right)}{\gamma_B^{1-2L_B\mu_B-2k}e^{\mathcal{A}_B\gamma_B}}\mathrm{d}\gamma_B, \quad (9)$$

where

$$\mathcal{A}_B = \frac{\mu_B(\eta_B+1)^2}{2\eta_B\bar{\gamma}_B}, \quad (10)$$

and

$$\mathcal{A}_E = \frac{\mu_E(\eta_E+1)^2}{2\eta_E\bar{\gamma}_E}. \quad (11)$$

By denoting the integral in (9) as $\mathcal{I}_1^{\eta}$, making use of [23, Eq. (8.352.4)], and carrying out after some algebraic manipulations, it follows that

$$\mathcal{I}_1^{\eta} = (2L_E\mu_E+2j-1)!\left\{\int_0^{\infty}\ln(1+\gamma_B)\gamma_B^{2L_B\mu_B+2k-1} \times e^{-\mathcal{A}_B\gamma_B}\mathrm{d}\gamma_B - \sum_{n=0}^{2L_E\mu_E+2j-1}\frac{1}{n!}\mathcal{A}_E^n \times \int_0^{\infty}\frac{\ln(1+\gamma_B)}{\gamma_B^{1-2L_B\mu_B-2k-n}}e^{-\mathcal{A}_B\gamma_B+\mathcal{A}_E\gamma_B}\mathrm{d}\gamma_B\right\}. \quad (12)$$

It is noticed that both integrals in (12) have the form: $\int_0^{\infty}\ln(1+x)x^a e^{-bx}\mathrm{d}x$, where $a>0$ and $b>0$. To this effect and using [26, Eq. (78)], the first integral of (12), denoted by $\mathcal{I}_{11}^{\eta}$, can be derived as

$$\mathcal{I}_{11}^{\eta} = \frac{\Gamma(2L_B\mu_B+2k)}{e^{-\mathcal{A}_B}} \times \sum_{m=1}^{2L_B\mu_B+2k}\frac{\Gamma\left(m-2L_B\mu_B-2k, \mathcal{A}_B\right)}{\mathcal{A}_B^m}. \quad (13)$$

Similarly, the second integral in (12) can be derived so that $\mathcal{I}_1^{\eta}$ can be expressed as in closed-form as follows:

$$\mathcal{I}_1^{\eta} = \Gamma(2L_E\mu_E+2j)\Big[\Gamma(2L_B\mu_B+2k)e^{\mathcal{A}_B} \times \sum_{m=1}^{2L_B\mu_B+2k}\frac{\Gamma\left(m-2L_B\mu_B-2k, \mathcal{A}_B\right)}{\mathcal{A}_B^m} \quad (14)$$

$$- \sum_{n=0}^{2L_E\mu_E+2j-1}\sum_{\iota=1}^{2L_B\mu_B+2k+n}\frac{\Gamma(2L_B\mu_B+2k+n)}{n!} \times \frac{\mathcal{A}_E^n e^{\mathcal{A}_B+\mathcal{A}_E}}{(\mathcal{A}_B+\mathcal{A}_E)^{\iota}}\Gamma\left(\iota-2L_B\mu_B-2k-n, \mathcal{A}_B+\mathcal{A}_E\right)\Big]. \quad (15)$$

Then, by replacing (15) into (9), an analytical expression for $\mathcal{J}_1^{\eta}$ can be obtained as (16), shown at the top of the next page (see p. 5), where $\Gamma(\cdot,\cdot)$ denotes the upper incomplete Gamma function [23, Eq. (8.350.2)]. Likewise, an expression for $\mathcal{J}_2^{\eta}$ can also be attained from (16) after replacing L_B by L_E, μ_B by μ_E, H_B by H_E, h_B by h_E, and $\bar{\gamma}_B$ by $\bar{\gamma}_E$, and vice-versa.

Next, by substituting appropriately (3) into the expression of $\mathcal{J}_3^{\eta}$ in (8), and using [26, Eq. (78)] along with some algebraic manipulations, $\mathcal{J}_3^{\eta}$ can be derived as

$$\mathcal{J}_3^{\eta} = \frac{2\sqrt{\pi}}{\ln(2)\Gamma(L_E\mu_E)}\left(\frac{(\eta_E+1)^2}{4\eta_E}\right)^{L_E\mu_E} \times \sum_{k=0}^{\infty}\frac{\mu_E^{2L_E\mu_E+2k}\Gamma(2L_E\mu_E+2k)}{k!\Gamma(L_E\mu_E+k+0.5)}\left(\frac{(\eta_E+1)^2}{4\eta_E}\right)^{2k} \times e^{\mathcal{A}_E}\sum_{m=1}^{2L_E\mu_E+2k}\frac{\Gamma\left(-2L_E\mu_E-2k+m, \mathcal{A}_E\right)}{(2\mu_E)^m\bar{\gamma}_E^{2L_E\mu_E+2k-m}}\mathcal{A}_E^{-2k}. \quad (17)$$

Therefore, by substituting (16) and (17) into (8) leads to the corresponding analytical expression for the $\bar{C}_S$ for the case of η-μ fading channels.

It is evident that the derived analytical expression for the $\bar{C}_S$ is expressed in terms of an infinite series representation. However, this is not a detrimental issue in practice since this series is fully convergent and it requires few terms to achieve sufficient levels of accuracy. In fact, fairly accurate results can be obtained by truncating the series after 50 terms, which yields a relative error due to truncation [27] of less than 0.002%. Also, the algebraic representation of the derived series is tractable since it consists of well-known elementary and special functions, which render it convenient to handle both analytically and numerically.

3.2 Exact ASC over λ-μ fading channels

Capitalizing on the derived analytical expression for the ASC over η-μ fading channels, we can also derive a similar expression for the ASC for the case of λ-μ fading channels. To this end, by substituting (4) and (6) into (8) and following the same process as in the previous subsection, it follows that

$$\mathcal{J}_1^{\lambda} = \frac{2\pi}{\ln(2)(1-\lambda_B^2)^{L_B\mu_B}\Gamma(L_B\mu_B)\Gamma(L_E\mu_E)} \times \sum_{k=0}^{\infty}\sum_{j=0}^{\infty}\frac{\lambda_B^{2k}\lambda_E^{2j}(1-\lambda_E^2)^{L_E\mu_E}}{k!j!(1-\lambda_B^2)^{2k}\bar{\gamma}_B^{2L_B\mu_B+2k}} \times \frac{2^{1-2L_E\mu_E-2j}\mu_B^{2L_B\mu_B+2k}}{\Gamma(L_B\mu_B+k+0.5)\Gamma(L_E\mu_E+2j+0.5)} \times \int_0^{\infty}\ln(1+\gamma_B)\gamma_B^{2L_B\mu_B+2k-1}e^{-\frac{2\mu_B\gamma_B}{\bar{\gamma}_B(1-\lambda_B^2)}} \times \gamma_{\text{inc}}\left(2L_E\mu_E+2j, \frac{2\mu_E\gamma_B}{(1-\lambda_E^2)\bar{\gamma}_E}\right)\mathrm{d}\gamma_B, \quad (18)$$

and

$$\mathcal{I}_1^{\lambda} = \Gamma(2L_E\mu_E+2j)\left\{\int_0^{\infty}\frac{\ln(1+\gamma_B)}{\gamma_B^{1-2L_B\mu_B-2k}}e^{-\frac{2\mu_B\gamma_B}{\bar{\gamma}_B(1-\lambda_B^2)}}\mathrm{d}\gamma_B - \sum_{n=0}^{2L_E\mu_E+2j-1}\frac{1}{n!}\left(\frac{2\mu_E}{\bar{\gamma}_E(1-\lambda_E^2)}\right)^n \times \int_0^{\infty}\frac{\ln(1+\gamma_B)}{\gamma_B^{1-2L_B\mu_B-2k-n}}e^{-\frac{2\mu_B\gamma_B}{\bar{\gamma}_B(1-\lambda_B^2)}-\frac{2\mu_E\gamma_B}{\bar{\gamma}_E(1-\lambda_E^2)}}\mathrm{d}\gamma_B\right\}, \quad (19)$$

$$\mathcal{J}_1^{\eta} = \frac{2\pi}{\ln(2)\Gamma(L_B\mu_B)\Gamma(L_E\mu_E)} \left(\frac{(\eta_B+1)^2}{4\eta_B}\right)^{L_B\mu_B} \times \sum_{k=0}^{\infty}\sum_{j=0}^{\infty} \frac{\mu_B^{2L_B\mu_B+2k}(2L_E\mu_E+2j-1)!}{k!j!2^{2L_E\mu_E+2j-1}\Gamma(L_B\mu_B+k+0.5)\Gamma(L_E\mu_E+j+0.5)} \left(\frac{1-\eta_B^2}{4\eta_B}\right)^{2k} \left(\frac{1-\eta_E^2}{4\eta_E}\right)^{2j} \left(\frac{4\eta_E}{(\eta_E+1)^2}\right)^{L_E\mu_E+2j} \times \Bigg[(2L_B\mu_B+2k-1)!e^{\mathcal{A}_B} \sum_{m=1}^{2L_B\mu_B+2k} \mathcal{A}_B^{-m}\Gamma\left(m-2L_B\mu_B-2k,\mathcal{A}_B\right) - \sum_{n=0}^{2L_E\mu_E+2j-1} \sum_{\iota=1}^{2L_B\mu_B+2k+n} \frac{1}{n!} \times\Gamma(2L_B\mu_B+2k+n)\mathcal{A}_E^n\left(\mathcal{A}_B+\mathcal{A}_E\right)^{-\iota} e^{\mathcal{A}_B+\mathcal{A}_E}\Gamma\left(-2L_B\mu_B-2k-n+\iota,\mathcal{A}_B+\mathcal{A}_E\right)\Bigg]. \quad (16)$$

$$\mathcal{J}_1^{\lambda} = \frac{2\pi(1-\lambda_E^2)^{L_E\mu_E}}{\ln(2)\Gamma(L_B\mu_B)\Gamma(L_E\mu_E)} \sum_{k=0}^{\infty}\sum_{j=0}^{\infty} \frac{\lambda_E^{2j}\lambda_B^{2k}\mu_B^{2L_B\mu_B+2k}2^{1-2L_E\mu_E-2j}\Gamma(2L_E\mu_E+2j)}{k!j!(1-\lambda_B^2)^{L_B\mu_B+2k}\Gamma(L_B\mu_B+k+0.5)\Gamma(L_E\mu_E+j+0.5)} \times \Bigg[\Gamma(2L_B\mu_B+2k)e^{\frac{2\mu_B}{\bar{\gamma}_B(1-\lambda_B^2)}} \sum_{m=1}^{2L_B\mu_B+2k} \left(\frac{\bar{\gamma}_B(1-\lambda_B^2)}{2\mu_B}\right)^m \Gamma\left(m-2L_B\mu_B-2k,\frac{2\mu_B}{\bar{\gamma}_B(1-\lambda_B^2)}\right) - \sum_{n=0}^{2L_E\mu_E+2j-1} \sum_{\iota=1}^{2L_B\mu_B+2k+n} \frac{1}{n!}\Gamma(2L_B\mu_B+2k+n) \left(\frac{2\mu_E}{\bar{\gamma}(1-\lambda_E^2)}\right)^n \left(\frac{2\mu_B}{\bar{\gamma}(1-\lambda_B^2)}+\frac{2\mu_E}{\bar{\gamma}(1-\lambda_E^2)}\right)^{-\iota} \times e^{\frac{2\mu_B}{\bar{\gamma}(1-\lambda_B^2)}} e^{\frac{2\mu_E}{\bar{\gamma}(1-\lambda_E^2)}} \Gamma\left(\iota-2L_B\mu_B-2k-n,\frac{2\mu_B}{\bar{\gamma}_B(1-\lambda_B^2)}+\frac{2\mu_E}{\bar{\gamma}_E(1-\lambda_E^2)}\right)\Bigg]. \quad (21)$$

which yields

$$\mathcal{I}_1^{\lambda} = \Gamma(2L_E\mu_E+2j)\Bigg[(2L_B\mu_B+2k-1)!e^{\frac{2\mu_B}{\bar{\gamma}_B(1-\lambda_B^2)}} \times \sum_{m=1}^{2L_B\mu_B+2k} \left(\frac{\bar{\gamma}_B(1-\lambda_B^2)}{2\mu_B}\right)^m \times\Gamma\left(m-2L_B\mu_B-2k,\frac{2\mu_B}{\bar{\gamma}_B(1-\lambda_B^2)}\right) - \sum_{n=0}^{2L_E\mu_E+2j-1} \sum_{\iota=1}^{2L_B\mu_B+2k+n} \frac{\Gamma(2L_B\mu_B+2k+n)}{n!} \frac{e^{\frac{2\mu_B}{\bar{\gamma}_B(1-\lambda_B^2)}}}{e^{-\frac{2\mu_E}{\bar{\gamma}_E(1-\lambda_E^2)}}} \times\Gamma\left(-2L_B\mu_B-2k-n+\iota,\frac{2\mu_B}{\bar{\gamma}_B(1-\lambda_B^2)}+\frac{2\mu_E}{\bar{\gamma}_E(1-\lambda_E^2)}\right) \times\left(\frac{2\mu_E}{\bar{\gamma}_E(1-\lambda_E^2)}\right)^n \left(\frac{2\mu_B}{\bar{\gamma}_B(1-\lambda_B^2)}+\frac{2\mu_E}{\bar{\gamma}_E(1-\lambda_E^2)}\right)^{-\iota}\Bigg]. \quad (20)$$

To this effect and after some long but basic algebraic manipulations, one obtains (21), at the top of this page. Likewise, an expression for $\mathcal{J}_2^{\lambda}$ can be deduced from (21) after replacing L_B by L_E, μ_B by μ_E, H_B by H_E, h_B by h_E, and $\bar{\gamma}_B$ by $\bar{\gamma}_E$, and vice-versa, whereas $\mathcal{J}_3^{\lambda}$ can be expressed as

$$\mathcal{J}_3^{\lambda} = \frac{2\sqrt{\pi}}{\ln(2)\Gamma(L_E\mu_E)(1-\lambda^2)^{L_E\mu_E}} \times \sum_{k=0}^{\infty} \frac{\lambda_E^{2k}\mu_E^{2L_E\mu_E+2k}\Gamma(2L_E\mu_E+2k)}{k!(1-\lambda_E^2)^{2k-m}\Gamma(L_E\mu_E+k+0.5)} \times \sum_{m=1}^{2L_E\mu_E+2k} \frac{\Gamma\left(m-2L_E\mu_E-2k,\frac{2\mu_E}{\bar{\gamma}_E(1-\lambda_E^2)}\right)}{\bar{\gamma}_E^{2L_E\mu_E+2k-m}e^{-\frac{2\mu_E}{\bar{\gamma}_E(1-\lambda_E^2)}}}. \quad (22)$$

Therefore, by substituting (21) and (22) into (8) and after some algebraic manipulations, the corresponding analytical expression for the $\bar{C}_S$ over $\lambda-\mu$ fading channels is deduced.

3.3 Upper Bounds for the Truncation Errors

As already mentioned, the derived expression for the ASC is given in terms of infinite series. Depending on the value of the involved parameters, this series requires different number of terms to ensure acceptable truncation that leads to accurate results. Unlike error rate measures that typically require several decimal digits accuracy, the derived ASC measure only requires, at most, a two-decimal digit accuracy. Nevertheless, even though the involved series achieves a sufficient accuracy for a relatively low number of terms, deriving a tight closed-form upper bound for the exact truncation error of this series will allow the determination of the exact accuracy for a specific number of terms at given scenarios. Based on this, we derive a tight and tractable closed-form upper bound for the truncation error of the derived series representation in (8). In this case, the truncation error of (8) can be bounded by deriving closed-form bounds for $\mathcal{J}_1^{\eta}$, $\mathcal{J}_2^{\eta}$ and $\mathcal{J}_3^{\eta}$, for the case of η-μ fading.

To this end, the truncation of $\mathcal{J}_1^{\eta}$ after $p-1$ terms results to the truncation error in (23), at the top of the next page, i.e., p. 6. It is evident that (23) can be upper bounded by (24), shown at the top of the next page (see p. 6). To this effect, we use the Pochhammer symbol identities in [28] and after some algebraic manipulations, the resulting expression with the two infinite series can be expressed in terms of the hypergeometric function [23], which yields a closed-form upper bound for $\mathcal{J}_1^{\eta}$. By following the same methodology, it follows that the upper bound of $\mathcal{J}_2^{\eta}$ can be also obtained in closed-form. The aforementioned two representations can be expressed in a more compact form as in (25), at the bottom of the next page (see p. 6), where the superscript "Tr" denotes *truncate*.

$$\mathcal{J}_1^{\eta} = \sum_{k=p}^{\infty}\sum_{j=p}^{\infty} \frac{\mu_B^{2k}(2L_E\mu_E+2j-1)!(1-\eta_E)^{2j}}{k!j!2^{2j}\Gamma(L_B\mu_B+k+\frac{1}{2})\Gamma(L_E\mu_E+j+\frac{1}{2})(1+\eta_E)^{2j}} \left(\frac{1-\eta_B^2}{4\eta_B}\right)^{2k} \times \Bigg[(2L_B\mu_B+2k-1)!e^{\mathcal{A}_B} \sum_{m=1}^{2L_B\mu_B+2k} \frac{\Gamma\left(-2L_B\mu_B-2k+m,\mathcal{A}_B\right)}{\mathcal{A}_B^m} - \sum_{n=0}^{2L_E\mu_E+2j-1}\sum_{i=1}^{2L_B\mu_B+2k+n} \frac{\Gamma(2L_B\mu_B+2k+n)\mathcal{A}_E^n}{n!(\mathcal{A}_B+\mathcal{A}_E)^i e^{-\mathcal{A}_B-\mathcal{A}_E}}\Gamma\left(-2L_B\mu_B-2k-n+i,\mathcal{A}_B+\mathcal{A}_E\right)\Bigg]. \tag{23}$$

$$\mathcal{J}_1^{\lambda} < \sum_{k=0}^{\infty} \frac{\lambda_B^{2k}\mu_B^{2k}}{k!(1-\lambda_B)^{2k}\Gamma(L_B\mu_B+k+\frac{1}{2})} \sum_{j=0}^{\infty} \frac{\lambda_E^{2j}\Gamma(2L_E\mu_E+2j)}{j!2^{2j}\Gamma(L_E\mu_E+j+\frac{1}{2})} \times \Bigg[\Gamma(2L_B\mu_B+2p)e^{\frac{2\mu_B}{\bar{\gamma}_B(1-\lambda_B^2)}} \sum_{m=1}^{2L_B\mu_B+2p} \left(\frac{\overline{\gamma}_B(1-\lambda_B^2)}{2\mu_B}\right)^m \Gamma\left(m-2L_B\mu_B-2p,\frac{2\mu_B}{\overline{\gamma}_B(1-\lambda_B^2)}\right) - \sum_{n=0}^{2L_E\mu_E+2j-1} \times \sum_{i=1}^{2L_B\mu_B+2p+n} \frac{\Gamma(2L_B\mu_B+2p+n)}{n!} \left(\frac{2\mu_E}{\bar{\gamma}_E(1-\lambda_E^2)}\right)^n e^{\frac{2\mu_B}{\bar{\gamma}_B(1-\lambda_B^2)}+\frac{2\mu_E}{\bar{\gamma}_E(1-\lambda_E^2)}} \times \left(\frac{2\mu_B}{\bar{\gamma}_B(1-\lambda_B^2)}+\frac{2\mu_E}{\bar{\gamma}_E(1-\lambda_E^2)}\right)^{-i} \Gamma\left(-2L_B\mu_B-2p-n+i,\frac{2\mu_B}{\bar{\gamma}_B(1-\lambda_B^2)}+\frac{2\mu_E}{\bar{\gamma}_E(1-\lambda_E^2)}\right)\Bigg]. \tag{24}$$

$$\left\{\begin{matrix}\mathcal{J}_1\\ \mathcal{J}_2\end{matrix}\right\}_{\mathrm{Tr}}^{\eta} \overset{\mathrm{k=j=p}}{<} \frac{\Gamma\left(2\left\{\begin{matrix}L_E\mu_E\\ L_B\mu_B\end{matrix}\right\}\right)}{\Gamma\left(L_B\mu_B+\frac{1}{2}\right)\Gamma\left(L_E\mu_E+\frac{1}{2}\right)} {}_0F_1\left(;\left\{\begin{matrix}L_B\mu_B\\ L_E\mu_E\end{matrix}\right\}+\frac{1}{2};\left\{\begin{matrix}\left(\frac{1-\eta_B^2}{4\eta_B}\right)^2\mu_B^2\\ \left(\frac{1-\eta_E^2}{4\eta_E}\right)^2\mu_E^2\end{matrix}\right\}\right) {}_1F_0\left(\left\{\begin{matrix}L_E\mu_E\\ L_B\mu_B\end{matrix}\right\};;\left\{\begin{matrix}(1-\eta_E)^2/(1+\eta_E)^2\\ (1-\eta_B)^2/(1+\eta_B)^2\end{matrix}\right\}\right) \times \Bigg[\left(2\left\{\begin{matrix}L_B\mu_B\\ L_E\mu_E\end{matrix}\right\}+2p-1\right)!e^{\left\{\begin{matrix}\mathcal{A}_B\\ \mathcal{A}_E\end{matrix}\right\}} \sum_{m=1}^{2\left\{\begin{matrix}L_B\mu_B\\ L_E\mu_E\end{matrix}\right\}+2p} \left(\left\{\begin{matrix}\mathcal{A}_B^{-1}\\ \mathcal{A}_E^{-1}\end{matrix}\right\}\right)^m \Gamma\left(-2\left\{\begin{matrix}L_B\mu_B\\ L_E\mu_E\end{matrix}\right\}-2p+m,2\left\{\begin{matrix}\mathcal{A}_B\\ \mathcal{A}_E\end{matrix}\right\}\right) - \sum_{n=0}^{2\left\{\begin{matrix}L_E\mu_E\\ L_B\mu_B\end{matrix}\right\}+2j-1} \sum_{i=1}^{2\left\{\begin{matrix}L_B\mu_B\\ L_E\mu_E\end{matrix}\right\}+2p+n} \frac{\Gamma(2\left\{\begin{matrix}L_B\mu_B\\ L_E\mu_E\end{matrix}\right\}+2p+n)}{n!} \frac{\mathcal{A}_E^n e^{\mathcal{A}_B+\mathcal{A}_E}}{(\mathcal{A}_B+\mathcal{A}_E)^i}\Gamma\left(-2\left\{\begin{matrix}L_B\mu_B\\ L_E\mu_E\end{matrix}\right\}-2p-n+i,\mathcal{A}_B+\mathcal{A}_E\right)\Bigg]. \tag{25}$$

Similarly, a closed-form upper bound for the truncation error of $\mathcal{J}_3^{\eta}$ can be derived as

$$\mathcal{J}_3^{\mathrm{Tr},\eta} < \frac{\mu_E^{2L_{\mu_E}}\Gamma(2L\mu_E)\,{}_1F_0\left(L\mu_E;;\left(2\mu_E\frac{1-\eta_E^2}{4\eta_E}\right)^2\right)}{\Gamma\left(L\mu_E+\frac{1}{2}\right)\bar{\gamma}^{2L\mu_E+2p}e^{-\mathcal{A}_E}} \times \sum_{m=1}^{2L_{\mu_E}+2p} \frac{2\bar{\gamma}^m\eta_E}{\mu_E^m(\eta_E+1)^2}\Gamma\left(-2L\mu_E-2p+m,\mathcal{A}_E\right). \tag{26}$$

Having derived closed-form upper bounds for the truncation error of the infinite series representation for the ASC over η-μ fading channels, we can readily deduce a similar expression for the truncation error of the ASC for the case of λ-μ fading channels. To this end, by following the same procedure and after long but basic algebraic manipulations, the closed-form bounds in (27) (top of the next page, i.e., p.7) and (28) are deduced

$$\mathcal{J}_3^{\mathrm{Tr},\lambda} < \frac{\mu_E^{2L\mu_E}\Gamma(2L\mu_E)e^{\frac{2\mu_E}{\bar{\gamma}_E(1-\lambda_E^2)}}}{\Gamma\left(L\mu_E+\frac{1}{2}\right)\bar{\gamma}^{2L\mu_E+2p}} {}_1F_0\left(L\mu_E;;\frac{4\mu_E^2\lambda_E^2}{(1-\lambda_E^2)^2}\right) \times \sum_{m=1}^{2L_{\mu_E}+2p} \frac{\bar{\gamma}^m(1-\lambda_E^2)^m}{(2\mu_E)^m}\Gamma\left(m-2L\mu_E-2p,\frac{2\mu_E}{\bar{\gamma}_E(1-\lambda_E^2)}\right). \tag{28}$$

The derived bounds for the considered ASC cases are tight and can be readily computed in popular software packages (such as MATHEMATICA and MATLAB) that include the involved elementary and special functions as built-in functions. Thus, the accuracy of the derived series can be determined precisely at any given case.

4 Secrecy Outage Probability

4.1 Exact SOP over η-μ fading channels

Having determined the ASC over η-μ and λ-μ fading channels, it is next assumed that Eve acts in a passive manner and therefore the CSI of the eavesdropper channel is not available at Alice. The secrecy outage probability arises as an important performance metric to evaluate the security performance in this scenario, and it is defined as the probability that the instantaneous secrecy

$$\begin{Bmatrix}\mathcal{J}_1\\ \mathcal{J}_2\end{Bmatrix}_{\mathrm{Tr}}^{\lambda} \overset{\mathrm{k=j=p}}{<} \frac{\Gamma\left(2\begin{Bmatrix}L_E\mu_E\\ L_B\mu_B\end{Bmatrix}\right)}{\Gamma\left(L_B\mu_B+\frac{1}{2}\right)\Gamma\left(L_E\mu_E+\frac{1}{2}\right)}\,{}_0F_1\left(;\begin{Bmatrix}L_B\mu_B\\ L_E\mu_E\end{Bmatrix}+\frac{1}{2};\begin{Bmatrix}\lambda_B^2\mu_B^2/(1-\lambda_B^2)^2\\ \lambda_E^2\mu_E^2/(1-\lambda_E^2)^2\end{Bmatrix}\right)\,{}_1F_0\left(\begin{Bmatrix}L_E\mu_E\\ L_B\mu_B\end{Bmatrix};;\begin{Bmatrix}\lambda_E^2\\ \lambda_B^2\end{Bmatrix}\right)$$
$$\times\Bigg[\Gamma\left(2\begin{Bmatrix}L_B\mu_B\\ L_E\mu_E\end{Bmatrix}+2p\right)e^{\begin{Bmatrix}2\mu_B/(\bar\gamma_B(1-\lambda_B^2))\\ 2\mu_E/(\bar\gamma_E(1-\lambda_E^2))\end{Bmatrix}}\sum_{m=1}^{2\begin{Bmatrix}L_B\mu_B\\ L_E\mu_E\end{Bmatrix}+2p}\left(\begin{Bmatrix}\overline{\gamma}_B(1-\lambda_B^2)/(2\mu_B)\\ \bar\gamma_E(1-\lambda_E^2)/(2\mu_E)\end{Bmatrix}\right)^m\Gamma\left(-2\begin{Bmatrix}L_B\mu_B\\ L_E\mu_E\end{Bmatrix}-2p+m,2\begin{Bmatrix}\mu_B/(\bar\gamma_B(1-\lambda_B^2))\\ \mu_E/(\bar\gamma_E(1-\lambda_E^2))\end{Bmatrix}\right)$$
$$-\sum_{n=0}^{2\begin{Bmatrix}L_E\mu_E\\ L_B\mu_B\end{Bmatrix}+2j-1}\sum_{i=1}^{2\begin{Bmatrix}L_B\mu_B\\ L_E\mu_E\end{Bmatrix}+2p+n}\frac{\Gamma(2\begin{Bmatrix}L_B\mu_B\\ L_E\mu_E\end{Bmatrix}+2p+n)}{n!}\left(\frac{2\mu_E}{\bar\gamma_E(1-\lambda_E^2)}\right)^n\left(\frac{2\mu_B}{\bar\gamma_B(1-\lambda_B^2)}+\frac{2\mu_E}{\bar\gamma_E(1-\lambda_E^2)}\right)^{-i}$$
$$\times e^{\frac{2\mu_B}{\bar\gamma_B(1-\lambda_B^2)}+\frac{2\mu_E}{\bar\gamma_E(1-\lambda_E^2)}}\Gamma\left(-2\begin{Bmatrix}L_B\mu_B\\ L_E\mu_E\end{Bmatrix}-2p-n+i,\frac{2\mu_E}{\bar\gamma_B(1-\lambda_B^2)}+\frac{2\mu_E}{\bar\gamma_E(1-\lambda_E^2)}\right)\Bigg]. \tag{27}$$

$$P_{\mathrm{out}}^{\eta}(R_S)=\frac{4\pi h_E^{L_E\mu_E}}{\Gamma(L_E\mu_E)\Gamma(L_B\mu_B)}\sum_{k=0}^{\infty}\sum_{j=0}^{\infty}\frac{2^{2j}\eta_B^{L_B\mu_B+2j}\mu_E^{2L_E\mu_E+2k}\left(1-\eta_E^2\right)^{2k}\left(1-\eta_B^2\right)^{2j}\Gamma(2L_B\mu_B+2j)\Gamma(2L_E\mu_E+2k)}{k!j!2^{4k}\eta_E^{2k}(\eta_B+1)^{2L_B\mu_B+4j}\Gamma\left(L_E\mu_E+k+0.5\right)\Gamma\left(L_B\mu_B+j+0.5\right)\bar\gamma_E^{2L_E\mu_E+2k}}$$
$$\times\left[\mathcal{A}_E^{-2L_E\mu_E-2k}-e^{(1-2^{R_S})\mathcal{A}_B}\sum_{m=0}^{2L_B\mu_B+2j-1}\sum_{\iota=0}^{m}\frac{(-1)^{m-\iota}2^{R_S\iota}}{m!}\binom{m}{\iota}\mathcal{A}_B^m\Psi\left(2L_E\mu_E+2k,\iota+2L_E\mu_E+2k+1;\mathcal{A}_E+\mathcal{A}_B\right)\right]. \tag{30}$$

$$\begin{aligned}P_{\mathrm{out}}^{\lambda}(R_S)=&\frac{2\pi}{\Gamma(L_E\mu_E)\Gamma(L_B\mu_B)(1-\lambda_E^2)^{L_E\mu_E}}\\&\times\sum_{k=0}^{\infty}\sum_{j=0}^{\infty}\frac{2^{1-2L_B\mu_B-2j}\mu_E^{2L_E\mu_E+2k}\lambda_B^{2j}(1-\lambda_B^2)^{L_B\mu_B}\Gamma(2L_B\mu_B+2j)\Gamma(2L_E\mu_E+2k)}{k!j!\Gamma\left(L_E\mu_E+k+0.5\right)\Gamma\left(L_B\mu_B+j+0.5\right)\bar\gamma_E^{2L_E\mu_E+2k}}\left(\frac{\lambda_E}{1-\lambda_E^2}\right)^{2k}\\&\times\Bigg[\left(\frac{\bar\gamma_E(1-\lambda_E^2)}{2\mu_E}\right)^{2L_E\mu_E+2k}-e^{(1-2^{R_S})\frac{2\mu_B}{\bar\gamma_B(1-\lambda_B^2)}}\sum_{m=0}^{2L_B\mu_B+2j-1}\sum_{\iota=0}^{m}\frac{(-1)^{m-\iota}2^{R_S\iota}}{m!}\binom{m}{\iota}\\&\times\left(\frac{2\mu_B}{\bar\gamma_B(1-\lambda_B^2)}\right)^m\Psi\left(2L_E\mu_E+2k,\iota+2L_E\mu_E+2k+1;\frac{2\mu_E}{\bar\gamma_E(1-\lambda_E^2)}+\frac{2\mu_B}{\bar\gamma_B(1-\lambda_B^2)}\right)\Bigg].\end{aligned} \tag{31}$$

capacity remains below a target rate denoted by R_S. This can be mathematically formulated as

$$P_{\mathrm{out}}(R_S)=\int_0^{\infty}f_{\gamma_E}(\gamma_E)F_{\gamma_B}\left(2^{R_S}(1+\gamma_E)-1\right)\mathrm{d}\gamma_E. \tag{29}$$

Therefore, by substituting (3) and (5) in (29), and with the aid of [23, Eq. (8.352.4)] and [23, Eq. (3.351.3)], the binomial expansion $(y-1)^a=\sum_{\chi=0}^{a}\binom{a}{\chi}(-1)^{a-\chi}y^{\chi}$, and [23, Eq. (9.211.1)], an exact SOP is derived in (30), shown at the top of this page. In this expression, $\Psi(\cdot,\cdot;\cdot)$ denotes the confluent hypergeometric function of the second kind defined by [23, Eq. (9.211.1)]. It is also worth noting that although (30) is expressed in terms of infinite series, this converges rapidly and steadily with only a few terms.

4.2 Exact SOP over λ-μ fading channels

Having derived an explicit expression for the outage exact SOP over η-μ fading channels can lead to the derivation of a similar analytical expression for the SOP over λ-μ fading channels. To this end, by performing the necessary variable transformation in (4) and (6) and substituting into (29) along with some algebraic manipulations yields the explicit analytical representation in (31), at the top of this page.

4.3 Upper Bounds for the Truncation Errors

In the previous section, we derived closed-form upper bounds for the truncation error of the infinite series representations for the ASC over η-μ and λ-μ fading channels. These bounds are tractable and they can determine the required number of terms for certain target accuracy. Based on this, similar closed-form upper bounds can be also derived for the truncation error of the derived SOP infinite series representations for the case of η-μ and λ-μ fading conditions. To this end and given that the algebraic representation of the series representations for the considered ASC and SOP scenarios are algebraically similar, we follow the same procedure in bounding the series which ultimately leads to the following simple upper bound

$$\begin{aligned}P_{\mathrm{out}}^{\mathrm{Tr},\eta}<&\frac{\Gamma(2L_B\mu_B)\Gamma(2L_E\mu_E)}{\Gamma\left(L_B\mu_B+\frac{1}{2}\right)\Gamma\left(L_E\mu_E+\frac{1}{2}\right)}\\&\times{}_1F_0\left(L_E\mu_E;;\frac{(1-\eta_E)^2\mu_E^2}{\bar\gamma_E^2\eta_E^2}\right)\\&\times{}_1F_0\left(L_B\mu_B;;\frac{(1-\eta_B)^2}{(1+\eta_B)^2}\right),\end{aligned} \tag{32}$$

for the truncation error of the SOP over η-μ fading channels.

Based on this, a similar closed-form upper bounds can be

$$P_{\text{out}}^{\infty,\eta}(R_S)=\sum_{m=0}^{\infty}\frac{\pi\bar{\gamma}_E^{2L_B\mu_B}\bar{\gamma}_B^{-2L_B\mu_B}\Gamma(2L_B\mu_B+2L_E\mu_E+2m)\mu_B^{2L_B\mu_B-1}(\eta_B+1)^{2L_B\mu_B}2^{2L_B\mu_BR_S-2m+1}\eta_E^{2L_B\mu_B+L_E\mu_E}}{m!L_B\Gamma(L_B\mu_B)\Gamma(L_E\mu_E)\Gamma\left(L_B\mu_B+\frac{1}{2}\right)\Gamma\left(L_E\mu_E+m+\frac{1}{2}\right)\eta_B^{L_B\mu_B}\mu_E^{2L_B\mu_B}\left(\eta_E+1\right)^{4L_B\mu_B+2L_E\mu_E}}. \tag{37}$$

deduced for the truncation error of the SOP under λ-μ fading conditions. Hence, by performing the necessary change of variables and after some algebraic manipulations, the following inequality is deduced

$$P_{\text{out}}^{\text{Tr},\lambda}<\frac{\Gamma(2L_B\mu_B)\Gamma(2L_E\mu_E)}{\Gamma\left(L_B\mu_B+\frac{1}{2}\right)\Gamma\left(L_E\mu_E+\frac{1}{2}\right)}\,{}_1F_0\left(L_B\mu_B;;\lambda_B^2\right)\times{}_1F_0\left(L_E\mu_E;;\frac{(2\lambda_E\mu_E)^2}{\bar{\gamma}_E^2(1-\lambda_E^2)^2}\right). \tag{33}$$

It is evident that the derived closed-form upper bounds in (32) and (33) are rather compact and tractable.

4.4 Simple Asymptotic SOP Representations

Capitalizing on the exact derived expressions for the SOP over η-μ and λ-μ fading channels, we can investigate their behavior at the high SNR regime in order to develop useful insights on the role of the involved parameters on the system performance. To this end, assuming $\bar{\gamma}_B\to\infty$ and fixed $\bar{\gamma}_E$[4], our aim is to find an approximate expression of $P_{\text{out}}(R_S)$ in the form [29] $P_{\text{out}}^{\infty}(R_S)\approx\mathcal{G}_c\bar{\gamma}_B^{-\mathcal{G}_d}$, where $\mathcal{G}_c$ represents the secrecy array gain and $\mathcal{G}_d$ denotes the secrecy diversity gain. The secrecy diversity gain is defined as [30]

$$\mathcal{G}_d\doteq-\lim_{\bar{\gamma}_B\to\infty}\frac{\log\left(P_{\text{out}}^{\infty}(R_S)\right)}{\log(\bar{\gamma}_B)}, \tag{34}$$

where $P_{\text{out}}^{\infty}(R_S)$ will be determined subsequently for both η-μ and λ-μ fading conditions. First, note that (29) can be approximated using the expression of the lower bound[5]

$$P_{\text{out}}^{\infty}(R_S)=\int_0^{\infty}f_{\gamma_E}(\gamma_E)F_{\gamma_B}(2^{R_S}\gamma_E)\mathrm{d}\gamma_E. \tag{35}$$

Next, an approximation for the CDF $F_{\gamma_B}(\gamma_E)$ will be derived since it is dependent on $\bar{\gamma}_B$. To this end, as the PDF in (3) is dominated by the term corresponding to $k=0$ in the summation, for $\bar{\gamma}_B\to\infty$, such expression can be used to obtain the corresponding CDF, i.e.,

$$F_{\gamma_B}(\gamma_E)\approx\frac{\sqrt{\pi}\mu_B^{2L_B\mu_B-1}(1+\eta_B)^{2L_B\mu_B}\gamma_E^{2L_B\mu_B}}{L_B\Gamma(L_B\mu_B)\Gamma(L_B\mu_B+0.5)(4\eta_B)^{L_B\mu_B}\bar{\gamma}_B^{2L_B\mu_B}}. \tag{36}$$

Finally, substituting (3) and (36) into the aforementioned approximated SOP expression and using [23, (Eq. 3.381.4)] along with some algebraic manipulations, the asymptotic SOP can be derived in (37), at the top of this page. It is evident that the secrecy diversity gain is given by $\mathcal{G}_d=2L_B\mu_B$, which provides useful insights on the effect of the involved key parameter on the overall system performance. To this effect and recalling the Pochhammer symbol identities and the properties of the hypergeometric functions as well as carrying out some algebraic manipulations, the following compact closed-form asymptotic expression can be deduced for the SOP over η-μ fading channels at the high SNR regime:

$$P_{\text{out}}^{\infty,\eta}(R_S)=\frac{\pi\Gamma(2L_B\mu_B+2L_E\mu_E)\eta_E^{2L_B\mu_B+L_E\mu_E}}{\Gamma\left(L_E\mu_E+\frac{1}{2}\right)(1+\eta_E)^{4L_B\mu_B+2L_E\mu_E}\eta_B^{L_B\mu_B}}\times\frac{\bar{\gamma}_E^{2L_B\mu_B}\mu_B^{2L_B\mu_B-1}2^{1+2L_B\mu_BR_S-2L_E\mu_E}(1+\eta_B)^{2L_B\mu_B}}{L_B\bar{\gamma}_B^{2L_B\mu_B}\mu_E^{2L_B\mu_B}\Gamma(L_B\mu_B)\Gamma(L_E\mu_E)\Gamma\left(L_B\mu_B+\frac{1}{2}\right)}\times{}_2F_1\left(L_B\mu_B+L_E\mu_E,L_B\mu_B+\mathcal{C}_1;\mathcal{C}_1;\mathcal{C}_2\right). \tag{38}$$

where $\mathcal{C}_1$ and $\mathcal{C}_2$ are constant values given by

$$\mathcal{C}_1=L_E\mu_E+\frac{1}{2}, \tag{39}$$

and

$$\mathcal{C}_2=\frac{(1-\eta_E)^2}{(1+\eta_E)^2}. \tag{40}$$

The above expression provides useful insights on the impact of the involved parameters on the overall system performance. Furthermore, it can be used to derive a similar expression for the SOP over λ-μ fading channels. Thus, by performing the necessary variable transformation and after some algebraic manipulations, the following closed-form expression is deduced

$$P_{\text{out}}^{\infty,\lambda}(R_S)=\frac{\Gamma(2L_B\mu_B+2L_E\mu_E)(1-\lambda_E^2)^{2L_B\mu_B+L_E\mu_E}}{\Gamma\left(L_E\mu_E+\frac{1}{2}\right)(1-\lambda_B^2)^{L_B\mu_B}}\times\frac{\pi\bar{\gamma}_E^{2L_B\mu_B}\mu_B^{2L_B\mu_B-1}2^{1-2L_B\mu_B(1-R_S)-2L_E\mu_E}}{L_B\bar{\gamma}_B^{2L_B\mu_B}\mu_E^{2L_B\mu_B}\Gamma(L_B\mu_B)\Gamma(L_E\mu_E)\Gamma\left(L_B\mu_B+\frac{1}{2}\right)}\times{}_2F_1\left(L_B\mu_B+L_E\mu_E,L_B\mu_B+L_E\mu_E+\frac{1}{2};\mathcal{C}_1;\lambda_E^2\right). \tag{41}$$

To the best of the authors knowledge, the above analytical expressions have not been previously reported in the open technical literature.

5 Numerical Results and Discussions

In this section, representative numerical examples are plotted along with Monte Carlo simulations to assess the accuracy of the derived mathematical results. Without loss of generality, it is assumed that $R_S=1$bit/s/Hz throughout the paper, unless otherwise stated. In this section, we present the ASC and SOP performance metrics for various values of the fading parameters η, λ and μ. It is worthwhile to recall that η represents the scattered-wave power ratio between the in-phase and quadrature components of the wireless signal within any one cluster and has real positive values, i.e., $0<\eta<\infty$. On the other hand, $-1<\lambda<1$ represents the correlation coefficient between the scattered-wave in-phase and quadrature components of any multipath cluster, while $\mu>0$ is the number of multipath clusters in both fading models.

Fig. 2 shows the average secrecy capacity for various number of antennas at Bob and Eve, and different fading parameters. It can

4. Intuitively, due to the high probability of successful eavesdropping, the diversity gain associated with the case wherein $\bar{\gamma}_E\to\infty$, is zero.

5. It has generally been shown that the lower bound of the SOP is in close agreement with the exact SOP over the entire SNR regime (see [11], [14] and the references therein). Since finding a solution for the lower bound of the SOP is easier than the exact SOP one, we use the former to derive our asymptotic expressions of the SOP at high SNR.

be seen that the analytical results are in good agreement with the Monte-Carlo simulations across all the scenarios, which verifies the validity of the derived expressions. Although the fading parameters for the main and eavesdropper links vary, we note that as the number of antennas at Eve increases, the ASC decreases. This is expected since a high number of antennas at Eve yields some antenna diversity and therefore a secure eavesdropping which can be detrimental to the security performance of the system.

In addition, different combinations of the fading parameters for the main and eavesdropper channels are considered. The ASC corresponding to $\eta_B = 1.6, \mu_B = 3$ and $\eta_E = 0.7, \mu_E = 0.5$ outperforms the other ASC performances corresponding to other fading parameters. This observation shows that the fading parameters affect the overall security performance of the underlying system. In the same context, Fig. 3 illustrates the achieved ASC for different antennas values under λ-μ fading conditions. It is shown that the number of antennas is critical also in this case as the achieved ASC doubles in the moderate and high SNR regimes when $L_B = 2$ is changed to $L_B = 8$ for fixed fading conditions and $L_E = 2$.

Fig. 4 illustrates the impact of η and μ fading parameters on the achieved ASC. It is evident that the power ratio of the in-phase and quadrature components of the wireless signal in the two paths affects the overall system performance even for a fixed number of used antennas. Particularly in the case of considerably higher η_E compared to η_B, a non-negligible ASC degradation occurs across all SNR regimes. Likewise, this is also the trend regarding the effects of the correlation between the scattered-wave in-phase and quadrature components in Fig. 5. It is noticed that changes of over 20% for fixed number of antennas. Therefore, the variations of the number of antennas along with the fading parameters η, λ and μ affect the achieved ASC levels significantly. Moreover, a performance comparison between the underlying system over η-μ, λ-μ and the one over Rayleigh fading channels is provided. It can be seen that there is a performance improvement or deterioration of the η-μ or λ-μ over the Rayleigh depending on the values the fading parameters of the generalized fading. For example, the ASC with $\eta_B = 1$, $\mu_B = 1.5$ and $\eta_E = 3$, $\mu_E = 0.5$ outperforms the ASC corresponding to the Rayleigh from medium to high-SNR regimes, while the ASC corresponding to $\eta_B = 4$, $\mu_B = 0.5$ and $\eta_E = 2$, $\mu_E = 1.5$ is outperformed by the one in the Rayleigh case. From these observations, one can infer the scenarios under which the generalized η-μ provides a better security performance with respect to the well-known fading models.

Fig. 6 and Fig. 7 demonstrate the effect of $\bar{\gamma}_E$ on the corresponding ASC performance for fixed fading conditions and two different antenna combinations. It is evident that the values of $\bar{\gamma}_E$ is, as expected, rather critical on the achieved ASC levels. For example, an over 20% ASC enhancement or degradation is observed when the value of $\bar{\gamma}_E$ decreases or increases, respectively at both severe and light fading conditions. Furthermore, it becomes evident that the value of $\bar{\gamma}_E$ is comparably crucial to the number of selected antennas at Bob and Eve.

The above behavior is also observed in Fig. 8 and Fig. 9, which demonstrate the SOP for the considered fading conditions. It is noticed that changing the value of $\bar{\gamma}_E$ typically leads to SOP variations of about an order of magnitude across all $\bar{\gamma}_B$ values. In addition, it is shown that high $\bar{\gamma}_B$ values can ensure acceptable SOP levels even at moderate to high $\bar{\gamma}_E$ values. Conversely, low $\bar{\gamma}_B$ values lead to dramatically poor performance even for low $\bar{\gamma}_E$ values since the achieved SOP is shown to lie around unity. Therefore, besides ensuring that $\bar{\gamma}_B$ must be considerably greater than $\bar{\gamma}_E$, it must be also ensured that the value of $\bar{\gamma}_B$ is not low since the corresponding SOP will be rather poor regardless of the value of $\bar{\gamma}_E$ and the number of antennas. These figures also exhibit the accuracy of the derived closed-form asymptotic expressions for the SOP, which exhibit a tight match with the respective exact results in both moderate and high $\bar{\gamma}_B$ regimes.

The behavior of the SOP over η-μ and λ-μ fading conditions is also illustrated in Fig. 10 and Fig. 11. It is evident that the derived secrecy diversity gain is confirmed, i.e., $\mathcal{G}_d = 2L_B\mu_B$. Moreover, it is verified, as in the ASC case, that for a fixed number of antennas at Bob, an increasing number of antennas at Eve reduces considerably the overall security performance, whereas an increasing number of antennas at Bob (for a fixed number of antennas at Eve), improves the overall system performance. Furthermore, since it has been shown that the diversity gain is a function of μ_B, an increasing value of μ_B yields a performance improvement. Fig. 12 shows the SOP performance for various target secrecy rates R_S in η-μ conditions. It can be noted that as R_S increases, the SOP increases due to the fact that the outage event is likely to occur. It is worth noting that the aforementioned behavior can also be seen for different fading parameters and number of antennas.

Fig. 13 shows the SOP versus $\bar{\gamma}_B$ for different values of the target secrecy rates R_S for some well-known fading distributions, i.e., One-sided Gaussian, Rayleigh and Nakagami-m. In this scenario, $L_B = 4$, $L_E = 2$, and $\bar{\gamma}_E = 10$ dB and it can be seen that under the Rayleigh distribution ($\eta_\iota \to 1$, $\mu_\iota = 0.5$), the results coincide with the ones in [31, Fig. 3]. Moreover, this figure depicts the SOP performance under the one-sided Gaussian and Nakagami-m with $m = 2$. It is noted that as R_S decreases, the SOP performance improves in all scenarios, which corroborates the results in Fig. 12.

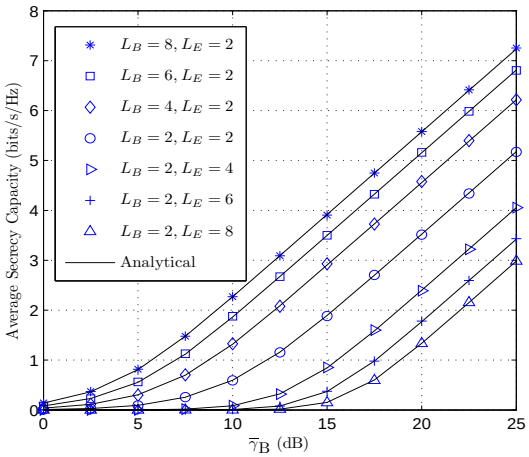

Fig. 2: Exact average secrecy capacity versus $\bar{\gamma}_B$ for different number of antennas and $\eta_B = 1.6$, $\mu_B = 2.5$, $\eta_E = 0.7$, $\mu_E = 0.5$ at $\bar{\gamma}_E = 10$ dB.

Finally, the overall impact of the involved different parameters on the overall performance under the effects of η-μ and λ-μ fading is demonstrated in Table 1, which depicts the corresponding ASC and the SOP for different values of η_B, η_E, μ_B, μ_E against L_B, L_E, $\bar{\gamma}_B$ and $\bar{\gamma}_E$ values. The two considered cases are analyzed for the following realistic scenarios: (a) severe η_B and μ_B with favorable η_E and μ_E; (b) favorable η_B and μ_B with severe η_E and μ_E;

TABLE 1: Effects of Fading parameters on the SOP and ASC for different system parameters.

Fading	System Parameters		$\bar{\gamma}_B$ (dB)	ASC (bits/s/Hz)	SOP
$\eta-\mu$ Fading Conditions	severe η_B-μ_B, light η_E-μ_E	$L_B=1,\ L_E=1$	15	3.81980	0.893285
			25	7.08452	0.021604
		$L_B=2,\ L_E=2$	15	4.31824	0.950617
			25	7.61596	0.001489
		$L_B=3,\ L_E=3$	15	4.51655	0.976031
			25	7.82320	0.000115
	light η_B-μ_B, severe η_E-μ_E	$L_B=1,\ L_E=1$	15	4.01385	0.815588
			25	7.29112	0.003253
		$L_B=2,\ L_E=2$	15	4.43691	0.909554
			25	7.73743	0.000073
		$L_B=3,\ L_E=3$	15	4.60384	0.952317
			25	7.91168	1.8091e-6
$\lambda-\mu$ Fading Conditions	severe λ_B-μ_B, light λ_E-μ_E	$L_B=1,\ L_E=1$	15	3.35750	0.864553
			25	6.41581	0.047707
		$L_B=2,\ L_E=2$	15	1.16424	0.692372
			25	4.55584	0.006152
		$L_B=3,\ L_E=3$	15	0.214783	0.371675
			25	1.441140	0.000886
	light λ_B-μ_B, severe λ_E-μ_E	$L_B=1,\ L_E=1$	15	3.84456	0.705777
			25	6.92600	0.001010
		$L_B=2,\ L_E=2$	15	3.24434	0.565260
			25	5.53814	5.7843e-8
		$L_B=3,\ L_E=3$	15	1.86507	0.295097
			25	3.09455	1.919e-13

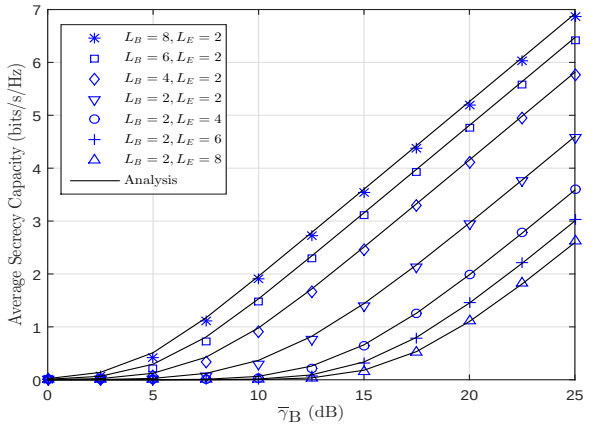

Fig. 3: Exact average secrecy capacity versus $\bar{\gamma}_B$ for different number of antennas and $\lambda_B = 0.4$, $\mu_B = 0.5$, $\lambda_E = 0.1$, $\mu_E = 1.5$ at $\bar{\gamma}_E = 10$ dB.

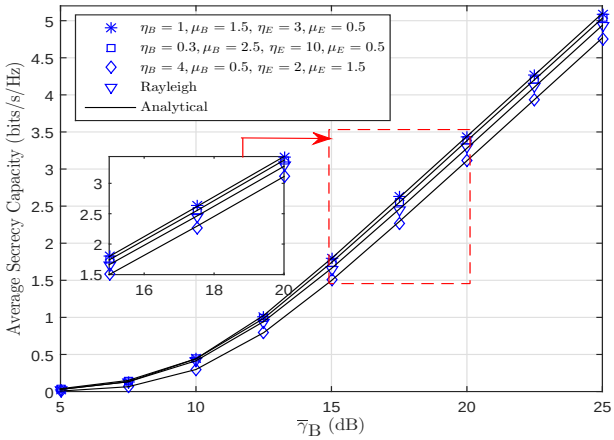

Fig. 4: Exact average secrecy capacity versus $\bar{\gamma}_B$ for different fading conditions and $L_B = 4$, $L_E = 4$ at $\bar{\gamma}_E = 10$ dB.

(c) severe λ_B and μ_B with favorable λ_E and μ_E; and (d) favorable λ_B and μ_B with severe λ_E and μ_E. Without loss of generality, the following parameters are used: $\bar{\gamma}_B = \{15\text{dB}, 25\text{dB}\}$ and $\eta_\iota = 4, \mu_\iota = 2$ (severe), $\eta_\iota = 1, \mu_\iota = 5$ (light or favorable) for the case of $\eta-\mu$ fading, where $\iota = \{B, E\}$, and $\lambda_\iota = 0.9, \mu_\iota = 2$ (severe) and $\lambda_\iota = 0.1, \mu_\iota = 5$ (favorable) for the case of λ-μ fading. In addition, we assume $\bar{\gamma}_E = 0$dB for the case of ASC and $\bar{\gamma}_E = 15$dB for the case of SOP. In this context, it is first verified that the ASC performance is affected by the different values of the fading parameters η_ι, λ_ι and μ_ι. For example, in the η-μ case, it can be noted that for various number of antennas or main link SNR values, the ASC under severe η_B, μ_B and light η_E, μ_E outperforms the one with favorable η_B, μ_B and severe η_E, μ_E. Similar observations are made for the case of λ-μ fading. Furthermore, as the number of antennas L_B and L_E increases, the ASC improves regardless of the scenario and the values of the main link SNR (e.g. 15dB, 25dB). More importantly, it is seen that in both cases and for any number of antennas, the ASC in scenario (b) outperforms the one in scenario (a). It is worth mentioning that, the performance difference between the two scenarios increases with the number of antennas between the corresponding values of the main link SNR.

In the same context, the effects of the fading parameters on the SOP are discussed. In the η-μ case, it can be seen that as the number of antennas increases, the SOP performance slightly deteriorates for $\bar{\gamma}_B = 15$dB. Intuitively, this can be explained as

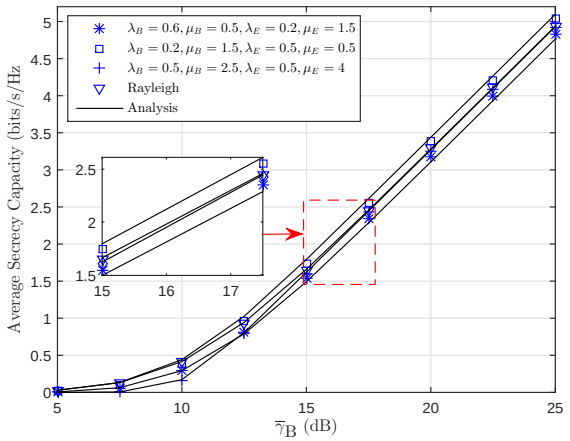

Fig. 5: Exact average secrecy capacity versus $\bar{\gamma}_{\mathrm{B}}$ for different fading conditions and $L_B = 4$, $L_E = 4$ at $\bar{\gamma}_{\mathrm{E}} = 10$ dB.

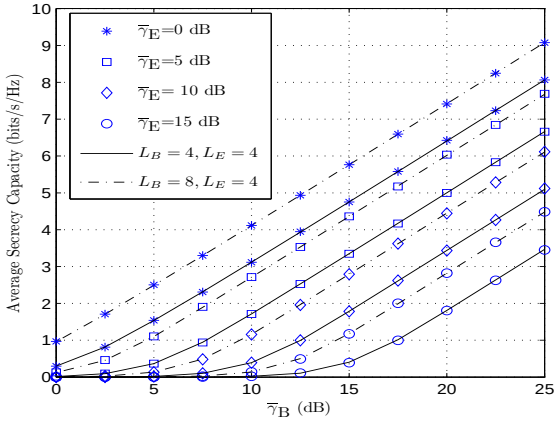

Fig. 6: Exact average secrecy capacity versus $\bar{\gamma}_{\mathrm{B}}$ for different $\bar{\gamma}_{\mathrm{E}}$ values and number of antennas for $\eta_B = 2.5$, $\mu_B = 3.5$, $\eta_E = 0.85$, $\mu_E = 0.5$.

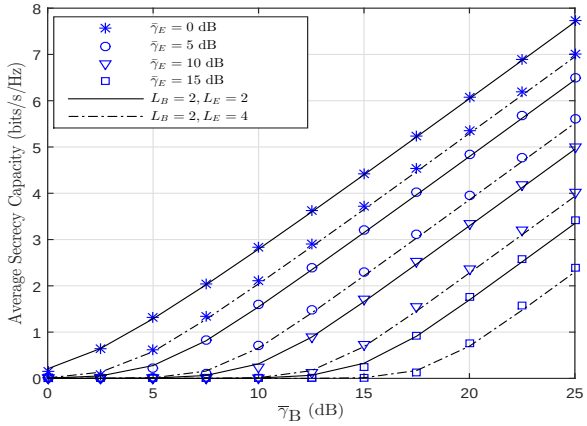

Fig. 7: Exact average secrecy capacity versus $\bar{\gamma}_{\mathrm{B}}$ for different $\bar{\gamma}_{\mathrm{E}}$ values number of antennas for $\lambda_B = 0.1$, $\mu_B = 2.5$, $\lambda_E = 0.1$, $\mu_E = 1.5$.

follows: the wiretap SNR is set to 15dB, i.e., the eavesdropper channel has the same quality as the main link. However, as the main link SNR improves (i.e., $\bar{\gamma}_B = 25$dB), a substantial performance improvement is noted as the number of antennas increases in both scenarios.

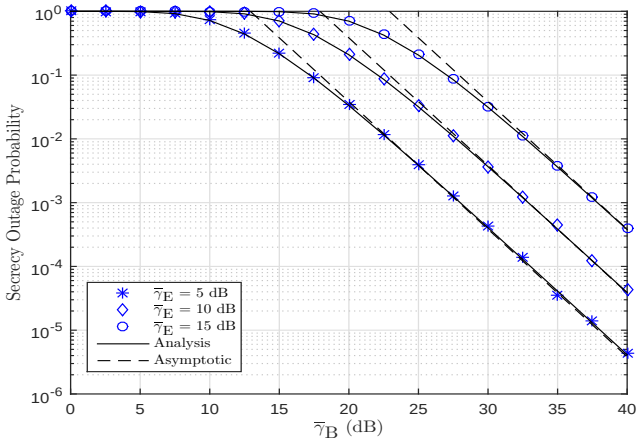

Fig. 8: Exact secrecy outage probability versus $\bar{\gamma}_{\mathrm{B}}$ for different $\bar{\gamma}_{\mathrm{E}}$ values and $\eta_B = 0.5$, $\mu_B = 0.5$, $\eta_E = 1.5$, $\mu_E = 2$, and system parameters $L_B = 2$, and $L_E = 4$.

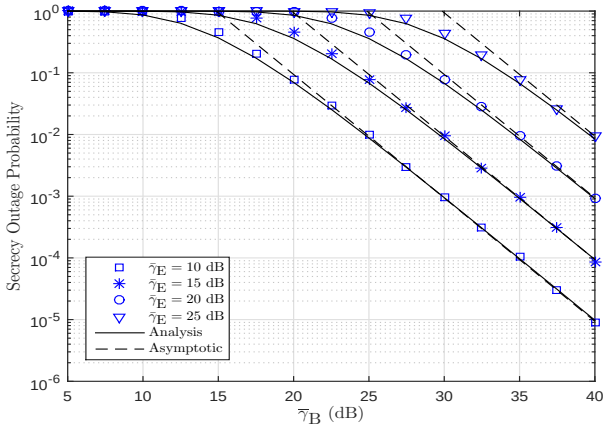

Fig. 9: Exact secrecy outage probability versus $\bar{\gamma}_{\mathrm{B}}$ for different $\bar{\gamma}_{\mathrm{E}}$ values and $\lambda_B = 0.2$, $\mu_B = 0.5$, $\lambda_E = 0.1$, $\mu_E = 2$, and system parameters $L_B = 2$, and $L_E = 2$.

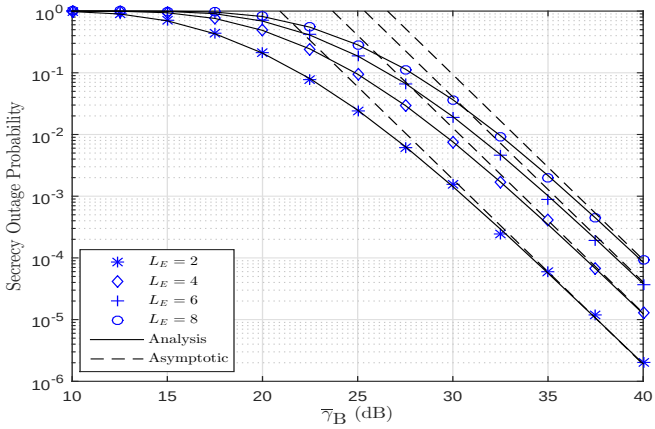

Fig. 10: Exact secrecy outage probability versus $\bar{\gamma}_{\mathrm{B}}$ for different L_E values and $\eta_B = 0.8$, $\mu_B = 1.5$, $\eta_E = 0.5$, $\mu_E = 2.5$, and $L_B = 1$ at $\bar{\gamma}_{\mathrm{E}} = 10$ dB.

As aforementioned, it is seen that η_ι, λ_ι and μ_ι have affect the PHY security of the underlying system. It is noted that such effects can be detrimental or can improve the system performance

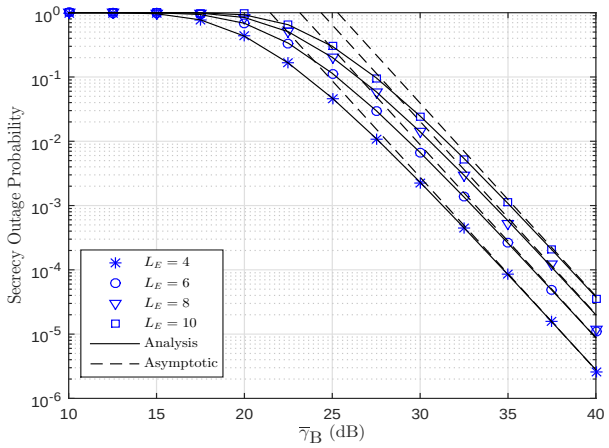

Fig. 11: Exact secrecy outage probability versus $\bar{\gamma}_{\mathrm{B}}$for different L_E values and $\lambda_B = 0.8$, $\mu_B = 1.5$, $\lambda_E = 0.5$, $\mu_E = 2.5$, and $L_B = 1$ at $\bar{\gamma}_{\mathrm{E}} = 10$ dB.

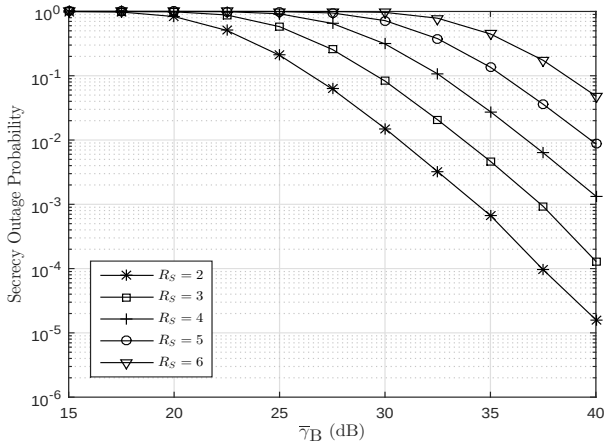

Fig. 12: Exact secrecy outage probability versus $\bar{\gamma}_{\mathrm{B}}$ for various secrecy target rates R_S. L_E values and $\lambda_B = 0.8$, $\mu_B = 1.5$, $\lambda_E = 0.5$, $\mu_E = 2.5$, and $L_B = 1$ at $\bar{\gamma}_{\mathrm{E}} = 10$ dB.

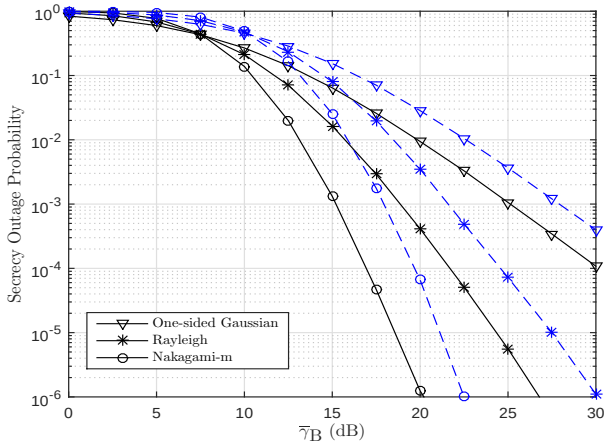

Fig. 13: Exact secrecy outage probability versus $\bar{\gamma}_{\mathrm{B}}$ for various well-known fading distributions. $L_B = 4$, $L_E = 2$ at $\bar{\gamma}_{\mathrm{E}} = 10$ dB. Solid lines correspond to $R_S = 0.1$ and dashed lines correspond to $R_S = 1$.

depending on the values of η_ι and μ_ι for the main and wiretap channels. The offered conclusions on the effects of the fading parameters on the system performance provide interesting insights that might be useful to future designs since the issue of security is addressed in this work.

6 Conclusions

This contribution addressed the secrecy performance of a wireless communication system over the generalized fading conditions characterized by the η-μ and λ-μ fading models. Novel analytical expressions were derived for the ASC and SOP, which have been validated through comparisons with respective results from Monte-Carlo simulations. Also, the asymptotic analysis for the SOP has shown to approximate well the exact SOP at the high SNR regime. The offered analytical results were then used in quantifying the effects of the different parameters on the achieved PHY layer security. It was shown that PHY depends significantly on these parameters, which verifies the need for accurate characterization and modeling of multipath fading conditions. Also, the offered results are expected to provide insights on the involved computational complexity and sustainability, since emerging communication systems are largely characterized by stringent quality of service and computational complexity requirements. Possible future extensions to this work involve multiple-input multiple-output (MIMO) wiretap channels with transmit antenna selection. MIMO systems have emerged as good candidates for current and future communication systems and therefore, its consideration in the context of physical later security is of paramount importance. Another direction of research could investigate the impact of outdated channel information in transmit antenna selection.

References

[1] X. Liu, "Probability of strictly positive secrecy capacity of the Rician-Rician fading channel," *IEEE Wireless Commun. Lett.,*, vol. 2, no. 1, pp. 50–53, Feb. 2013.

[2] X. Liu, "Outage probability of secrecy capacity over correlated lognormal fading channels," *IEEE Commun. Lett.*, vol. 17, no. 2, pp. 289–292, Feb. 2013.

[3] X. Liu, "Probability of strictly positive secrecy capacity of the Weibull fading channel," in *Proc. Global Communications Conference (GLOBECOM'13)*, Atlanta, GA, USA, Dec. 2013, pp. 659-664.

[4] X. Liu, "Secrecy capacity of wireless links subject to log-normal fading," in *Proc. International Conference on Communications and Networking in China (CHINACOM'12)*, Kunming, China, Aug. 2012, pp. 167-172.

[5] X. Liu, "Strictly positive secrecy capacity of log-normal fading channel with multiple eavesdroppers," in *Proc. IEEE International Conference on Communications (ICC'14)*, Sydney, NSW, Australia, Jun. 2014, pp. 775-779.

[6] M. Kamel, W. Hamouda and A. Youssef, "Physical layer security in ultra-dense networks," *IEEE Wireless Commun. Lett.*, vol. 6, no. 5, pp. 690–693, Oct. 2017.

[7] M. D. Yacoub, "The α-μ distribution: a physical fading model for the Stacy distribution," IEEE Trans. Veh. Technol., vol. 56, no. 1, pp. 2734, Jan. 2007.

[8] M. D. Yacoub, "The η-μ distribution and the κ-μ distribution," *IEEE Antennas Propag. Mag.*, vol. 49, no. 1, pp. 68–81, Feb. 2007.

[9] H. Lei, C. Gao, Y. Guo, and G. Pan, "On physical layer security over generalized Gamma fading channels," *IEEE Commun. Lett.*, vol. 19, no. 7, pp. 1257–1260, Jul. 2015.

[10] H. Lei, H. Zhang, I. S. Ansari, C. Gao, Y. Guo, G. Pan, and K. A. Qaraqe, "Performance analysis of physical layer security over generalized-K fading channels using a mixture Gamma distribution," *IEEE Commun. Lett.*, vol. 20, no. 2, pp. 408–411, Feb. 2016.

[11] N. Bhargav, S. L. Cotton, and D. E. Simmons, "Secrecy capacity analysis over κ-μ fading channels: theory and applications," *IEEE Trans. Commun.*, vol. 64, no. 7, pp. 3011–3024, Jul. 2016.

[12] H. Lei, I. S. Ansari, G. Pan, B. Alomair, and M.S. Alouini, "Secrecy capacity analysis over κ-μ fading channels," *IEEE Commun. Lett.*, vol. 21, no. 6, pp. 1445–1448, Jun. 2017.

[13] H. Lei, C. Gao, I. S. Ansari, Y. Guo, G. Pan, and K. A. Qaraqe, "On physical-layer security over SIMO generalized-K fading channels," *IEEE Trans. Veh. Technol.*, vol. 65, no. 9, pp. 7780–7785, Sep. 2016.

[14] J. M. Moualeu and W. Hamouda, "On the secrecy performance analysis of SIMO systems over κ-μ fading channels," *IEEE Commun. Lett.*, vol. 21, no. 11, pp. 2544–2547, Nov. 2017.

[15] M. Srinivasan and S. Kalyani, "Secrecy Capacity of κ-μ Shadowed Fading Channels," *IEEE Commun. Lett.*, vol. 22, no. 8, pp. 1728–1731, Aug. 2018.

[16] L. Kong, G. Kaddoum, and Z. Rezki, "Highly accurate and asymptotic analysis on the SOP over SIMO α-μ fading channels," *IEEE Commun. Lett.*, vol. 22, no. 10, pp. 2088–2091, Oct. 2018.

[17] L. Kong, S Vuppala, and G Kaddoum, "Secrecy analysis of random MIMO wireless networks over α-μ fading channels," *IEEE Trans Veh. Technol.*, 2018, DOI: 10.1109/TVT.2018.2872884.

[18] A. Mathur, Y. Ai, M. R. Bhatnagar, M. Cheffena, and T. Ohtsuki, "On physical layer security of α-η-κ-μ fading channels," *IEEE Commun. Lett.*, vol. 22, no. 10, pp. 2168–2171, Oct. 2018.

[19] M. D. Yacoub, "The α-η-κ-μ fading model," *IEEE Trans. Antennas Propag.*, vol. 64, no. 8, pp. 3597–3610, Aug. 2016.

[20] G. Fraidenraich, and M. D. Yacoub, "The $\lambda - \mu$ general fading distribution," *in Proc. SMBO/IEEE MTT-S IMOC*, Foz do Iguau, Brazil, Sep. 2003, pp. 49–54.

[21] J. F. Paris, P. C. Sofotasios, and T. A. Tsiftsis, "Special issue on advances in statistical channel modeling for wireless communications," *Hindawi Int. J. Ant. Propag.*, vol. 2015, Art. no. 541619.

[22] P. C. Sofotasios, S. Muhaidat, M. Valkama, M. Ghogho, and G. K. Karagiannidis, "Entropy and channel capacity under optimum power and rate adaptation over generalized fading conditions," *IEEE Signal Process. Lett.*, vol. 22, no. 11, pp. 2162–2166, Nov. 2015.

[23] I. S. Gradshteyn and I. M. Ryzhik, *Table of Integrals, Series, and Products*, 7th ed., San Diego, CA: Academic, 2007.

[24] K. Peppas, F. Lazarakis, A. Alexandridis, and K. Dangakis, "Error performance of digital modulation schemes with MRC diversity reception over η-μ fading channels," *IEEE Trans. Wireless Commun.*, vol. 8, no. 10, pp. 4974–4980, Oct. 2009.

[25] L. Wang, M. Elkashlan, J. Huang, R. Schober, and R. Mallik, "Secure transmission with antenna selection in MIMO Nakagami-m fading channels," *IEEE Trans. Wireless Commun.*, vol. 13, no. 11, pp. 6054–6067, Nov. 2014.

[26] M.-S. Alouini and A. Goldsmith, "Capacity of Rayleigh fading channels under different adaptive transmission and diversity-combining techniques," *IEEE Trans. Veh. Technol.*, vol. 48, no. 4, pp. 1165–1181, Jul. 1999.

[27] W. Zhao, G. Wang, S. Atapattu, C. Tellambura, and H. Guan, "Outage analysis of ambient backscatter communication systems," *IEEE Commun. Lett.*, vol. 22, no. 8, pp. 1736-1739, Aug. 2018.

[28] P. C. Sofotasios, T. A. Tsiftsis, Yu. A. Brychkov, S. Freear, M. Valkama, and G. K. Karagiannidis, "Analytic expressions and bounds for special functions and applications in communication theory," *IEEE Trans. Inf. Theory*, vol. 60, no. 12, pp. 7798–7823, Dec. 2014.

[29] N. Yang, P. L. Yeoh, M. Elkashlan, R. Schober, and I. B. Collings, "Transmit antenna selection for security enhancement in MIMO wiretap channels," *IEEE Trans. Commun.*, vol. 61, no. 1, pp. 144–154, Jan. 2013.

[30] Y. Liu, Z. Qin, M. Elkashlan, Y. Gao, and L. Hanzo, "Enhancing the physical layer security of non-orthogonal multiple access in large-scale networks," *IEEE Trans. Wireless Commun.*, vol. 16, no. 3, pp. 1656–1672, Mar. 2017.

[31] F. He, H. Man, and W. Wang, "Maximal ratio diversity combining enhanced security," *IEEE Commun. Lett.*, vol. 15, no. 5, pp. 509511, May 2011.

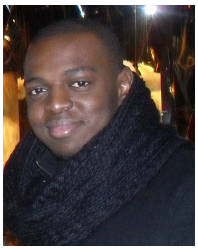

Jules M. Moualeu (S'06-M'14-SM'18) received the M.Sc.Eng. and Ph.D. degrees in electronic engineering from the University of KwaZulu-Natal, Durban, South Africa, in 2008 and 2013, respectively. During his PhD studies, he was a Visiting Scholar at Concordia University, Montreal, Canada, under the Canadian Commonwealth Scholarship Program (CCSP) offered by the Foreign Affairs and International Trade Canada (DFAIT). He joined the Department of Electrical and Information Engineering, University of the Witwatersrand, Johannesburg, South Africa, in 2015, and is also an affiliate Assistant Professor at Concordia University. He is currently an NRF Y-Rated Researcher and his current research interests include cooperative and relay communications, cognitive radio networks, energy harvesting, multiple-input multiple-output systems, non-orthogonal multiple access schemes, and physical-layer security. He received the Exemplary Reviewer Certificate of the IEEE COMMUNICATIONS LETTERS in 2018.

Paschalis C. Sofotasios (S'07-M'12-SM'16) was born in Volos, Greece, in 1978. He received the M.Eng. degree from Newcastle University, U.K., in 2004, the M.Sc. degree from the University of Surrey, U.K., in 2006, and the Ph.D. degree from the University of Leeds, U.K., in 2011. He has held academic positions at the University of Leeds, U.K., University of California at Los Angeles, CA, USA, Tampere University of Technology, Finland, Aristotle University of Thessaloniki, Greece and Khalifa University of Science and Technology, UAE, where he currently serves as Assistant Professor in the department of Electrical and Computer Engineering. His M.Sc. studies were funded by a scholarship from UK-EPSRC and his Doctoral studies were sponsored by UK-EPSRC and Pace plc. His research interests are in the broad areas of digital and optical wireless communications as well as in topics relating to special functions and statistics. Dr. Sofotasios serves as a regular reviewer for several international journals and has been a member of the technical program committee of numerous IEEE conferences. He currently serves as an Editor for the IEEE COMMUNICATIONS LETTERS and he received the Exemplary Reviewer Award from the IEEE COMMUNICATIONS LETTERS in 2012 and the IEEE TRANSACTIONS ON COMMUNICATIONS in 2015 and 2016. Dr. Sofotasios is a Senior Member IEEE and he received the Best Paper Award at ICUFN 2013.

Daniel B. da Costa (S'04-M'08-SM'14) was born in Fortaleza, Ceará, Brazil, in 1981. He received the B.Sc. degree in Telecommunications from the Military Institute of Engineering (IME), Rio de Janeiro, Brazil, in 2003, and the M.Sc. and Ph.D. degrees in Electrical Engineering, Area: Telecommunications, from the University of Campinas, SP, Brazil, in 2006 and 2008, respectively. His Ph.D thesis was awarded the Best Ph.D. Thesis in Electrical Engineering by the Brazilian Ministry of Education (CAPES) at the 2009 CAPES Thesis Contest. From 2008 to 2009, he was a Postdoctoral Research Fellow with INRS-EMT, University of Quebec, Montreal, QC, Canada. Since 2010, he has been with the Federal University of Ceará, where he is currently an Associate Professor.

Prof. da Costa is currently Senior Editor of the IEEE COMMUNICATIONS LETTERS and Editor of the IEEE COMMUNICATIONS SURVEYS AND TUTORIALS, IEEE TRANSACTIONS ON COMMUNICATIONS, IEEE TRANSACTIONS ON VEHICULAR TECHNOLOGY, IEEE ACCESS, IEEE TRANSACTIONS ON COGNITIVE COMMUNICATIONS AND NETWORKING, and EURASIP JOURNAL ON WIRELESS COMMUNICATIONS AND NETWORKING. He has also served as Associate Technical Editor of the IEEE COMMUNICATIONS MAGAZINE. From 2012 to 2017, he was Editor of the IEEE COMMUNICATIONS LETTERS. He has served as Area Editor of KSII TRANSACTIONS ON INTERNET AND INFORMATION SYSTEMS and as Guest Editor of several Journal Special Issues. He has been involved on the Organizing Committee of several conferences. He is currently the Latin American Chapters Coordinator of the IEEE Vehicular Technology Society. Also, he acts as a Scientific Consultant of the National Council of Scientific and Technological Development (CNPq), Brazil, and he is a Productivity Research Fellow of CNPq. Currently, he is Vice-Chair of Americas of the IEEE Technical Committee of Cognitive Networks (TCCN), Director of the TCCN Newsletter, and Chair of the Special Interest Group on Energy-Harvesting Cognitive Radio Networks in IEEE TCCN.

Prof. da Costa is the recipient of four conference paper awards. He received the Exemplary Reviewer Certificate of the IEEE WIRELESS COMMUNICATIONS LETTERS in 2013, the Exemplary Reviewer Certificate of the IEEE COMMUNICATIONS LETTERS in 2016 and 2017, the Certificate of Appreciation of Top Associate Editor for outstanding contributions to IEEE TRANSACTIONS ON VEHICULAR TECHNOLOGY in 2013, 2015 and 2016, the Exemplary Editor Award of IEEE COMMUNICATIONS LETTERS in 2016, and the Outstanding Editor Award of IEEE ACCESS in 2017. He is a Distinguished Lecturer of the IEEE Vehicular Technology Society. He is a Senior Member of IEEE, Member of IEEE Communications Society and IEEE Vehicular Technology Society.

Sami Muhaidat (S'01-M'08-SM'11) received the Ph.D. degree in electrical and computer engineering from the University of Waterloo, Waterloo, ON, Canada, in 2006. From 2007 to 2008, he was an NSERC Post-Doctoral Fellow with the Department of Electrical and Computer Engineering, University of Toronto, ON, Canada. From 2008 to 2012, he was Assistant Professor with the School of Engineering Science, Simon Fraser University, Burnaby, BC, Canada. He is currently an Associate Professor with Khalifa University, Abu Dhabi, UAE, and a Visiting Professor with the Department of Electrical and Computer Engineering, University of Western Ontario, London, ON, Canada. He is also a Visiting Reader with the Faculty of Engineering, University of Surrey, Guildford, U.K. Dr. Muhaidat currently serves as an Area Editor of the IEEE TRANSACTIONS ON COMMUNICATIONS, and he was previously a Senior Editor of the IEEE COMMUNICATIONS LETTERS and an Associate Editor of IEEE TRANSACTIONS ON COMMUNICATIONS, IEEE COMMUNICATIONS LETTERS and IEEE TRANSACTIONS ON VEHICULAR TECHNOLOGY. He was a recipient of several scholarships during his undergraduate and graduate studies and the winner of the 2006 NSERC PostDoctoral Fellowship Competition. Dr Muhaidat is a Senior Member IEEE.

Walaa Hamouda (S'97-M'02-SM'06) received the M.A.Sc. and Ph.D. degrees in electrical and computer engineering from Queen's University, Kingston, ON, Canada, in 1998 and 2002, respectively. Since July 2002, he has been with the Department of Electrical and Computer Engineering, Concordia University, Montreal, QC, Canada, where he is currently a Professor. Since June 2006, he has been a Concordia University Research Chair in Communications and Networking. His current research interests include single/multiuser multiple-input-multiple-output communications, space-time processing, cooperative communications, wireless networks, multiuser communications, cross-layer design, and source and channel coding.

Dr. Hamouda served as the Technical Co-chair of the Fifth International Conference on Selected Topics in Mobile & Wireless Networking (MoWNet'16), Track Co-Chair: Multiple Antenna and Cooperative Communications, IEEE Vehicular Technology Conference (VTC-Fall16), Co-Chair: ACM Performance Evaluation of Wireless Ad Hoc, Sensor, and Ubiquitous Networks (ACM-PE-WASUN), Co-chair of the Wireless Networks Symposium, 2012 Global Communications Conference; the Ad-hoc, Sensor, and Mesh Networking Symposium of the 2010 ICC; and the 25th Queen's Biennial Symposium on Communications. He also served as the Track Co-chair of Radio Access Techniques of the Fall 2006 IEEE Vehicular Technology Conference (VTC) and the Transmission Techniques of the Fall 2012 IEEE VTC. From September 2005 to November 2008, he was the Chair of the IEEE Montreal Chapter in Communications and Information Theory. He has received numerous awards, including the Best Paper Award at ICC 2009 and the IEEE Canada Certificate of Appreciation in 2007 and 2008. He served as an Associate Editor for the IEEE COMMUNICATIONS LETTERS and the IEEE TRANSACTIONS ON SIGNAL PROCESSING. He currently serves as an Associate Editor for the IEEE TRANSACTIONS ON VEHICULAR TECHNOLOGY, an editor for IEEE COMMUNICATIONS SURVEYS TUTORIALS, and IEEE WIRELESS COMMUNICATIONS LETTERS.

Ugo S. Dias (S'04-M'08-SM'18) was born in Belém, Pará, Brazil, in 1981. He received the B.Sc. degree in Electrical Engineering from the Federal University of Pará, Brazil, in 2004, and the M.Sc. and Ph.D. degrees in Electrical Engineering, Area: Telecommunications, from the University of Campinas, Brazil, in 2006 and 2010, respectively. Since March 2010, Dr. Ugo Dias is an Assistant Professor at University of Brasilia (UnB), Brazil. He is a faculty member of the Department of Electrical Engineering, Latitude and MWSL Labs. His main research interests include fading channels, field measurements, coexistence and quality of experience for future wireless networks, and wireless technologies in general.

Prof. Dias is currently Editor of the IET ELECTRONICS LETTERS and ACTA PRESS - COMMUNICATIONS. He has been involved on the Organizing Committee of several conferences. He is the recipient of four conference paper awards and one award from IEEE R9 for "the First Place in the IEEE R9 Success Story Contest - ComSoc Student Chapter 2017. Besides the academic experiences, he also worked in several companies in the ICT industry. Currently, Prof. Dias serves as Vice President of the Brazilian Telecommunications Society, chair of the IEEE ComSoc CN Brazil Chapter, and advisor of the IEEE ComSoc UnB Student Branch Chapter. He is a Senior Member of IEEE and Brazilian Telecommunications Society, and Member of IEEE Communications Society and Brazilian Communications Committee.